Mon. Not. R. Astron. Soc. **000**, 000–000 (0000) Printed 5 February 2008 (MN LATEX style file v1.4)

The Cluster Distribution as a Test of Dark Matter Models. III: The Cluster Velocity Field

L. Moscardini[1], E. Branchini[2,3], P. Tini Brunozzi[4,5], S. Borgani[2,5], M. Plionis[2,6] & P. Coles[7]

[1] *Dipartimento di Astronomia, Università di Padova, vicolo dell'Osservatorio 5, I–35122 Padova, Italy*

[2] *SISSA – International School for Advanced Studies, via Beirut 2–4, I–34013 Trieste, Italy*

[3] *Department of Physics, University of Durham, South Road, Durham DH1 3LE, UK*

[4] *Dipartimento di Fisica, Università di Perugia, via A. Pascoli, I–06100 Perugia, Italy*

[5] *INFN Sezione di Perugia, c/o Dipartimento di Fisica dell'Università, via A. Pascoli, I–06100 Perugia, Italy*

[6] *National Observatory of Athens, Lofos Nimfon, Thesio, 18110 Athens, Greece*

[7] *Astronomy Unit, School of Mathematical Sciences, Queen Mary & Westfield College, Mile End Road, London E1 4NS, UK*

5 February 2008

ABSTRACT

We study the large–scale velocity fields traced by galaxy clusters in numerical simulations of a box of side 960 h^{-1} Mpc, and compare them with available data on real clusters. In order to test the reliability of the simulations, which are based on an optimized version of the Zel'dovich approximation, we compare their cluster velocities with those of "exact" N–body simulations, and find a remarkable agreement between the two according to a variety of statistical tests. We analyse Cold Dark Matter (CDM) models with density parameter in the range $0.2 \leq \Omega_0 \leq 1$, both with and without the cosmological constant term to provide a flat geometry. We also simulate a Cold+Hot Dark Matter (CHDM) model, with 30% provided by the hot component. Comparison with real data is performed by applying tests based on the cumulative velocity frequency distribution (CVFD) and bulk flow statistics. For the CVFD, we use observational velocity data from different authors. By merging all available data in a combined sample, the CVFD test is able to exclude only open models with $\Omega_0 \leq 0.4$ and flat models with $\Omega_0 = 0.2$. However, the analysis of individual observational samples gives contradictory results; in particular the recent Giovanelli (1995) data, which imply much lower velocities (with significantly smaller uncertainties) than the other data, are actually only consistent with the open $\Omega_0 = 0.4$ and the flat $\Omega_0 = 0.2$ models, i.e. the models which are excluded by the other data. Furthermore, CVFD and bulk flow analyses of the Branchini et al. (1995) reconstructed velocity data disfavour precisely those models accepted on the grounds of Giovanelli's sample. Finally, we confirm that the Lauer & Postman (1994) bulk flow determination is an extremely rare event in the cosmological models we have analysed.

Key words: Cosmology: theory – dark matter – galaxies: clustering, formation – large–scale structure of Universe

1 INTRODUCTION

The quality and quantity of galaxy peculiar velocity data derived from the Infra–Red Tully–Fisher (IRTF) and D_n–σ scaling relations is progressively increasing, providing an ever more precise description of large–scale cosmic flows. Moreover, an independent technique to estimate the distance of high redshift galaxies with very small errors, based on the shapes of type Ia supernova light curves, recently developed by Riess, Press & Kirshner (1995), could allow a description of motions on even larger scales. Consequently the study of large–scale flows is potentially one of the most powerful tools with which to understand the structure of the universe on large ($\gtrsim 50\,h^{-1}$ Mpc) scales (see reviews by Dekel 1994; Strauss & Willick 1995 and references therein). Furthermore, the hypothesis of gravitational instability allows one to relate the peculiar velocity field directly to the entire mass distribution, under the plausible assumption that at such large scales galaxies share the same dynamics as the dark matter distribution.

Clusters of galaxies provide a particularly efficient and precise way to estimate peculiar motions, since the determination of many redshift–independent distances of cluster members leads to a substantial reduction in the statistical errors compared to studies of isolated galaxies. Moreover, new techniques based on the Sunyaev–Zel'dovich (1980) effect (Haenhelt & Tegmark 1995) and on the brightest cluster galaxy distance indicator method (Lauer & Postman 1994) are beginning to provide independent estimates of cluster peculiar velocities whose reliability is expected to increase considerably in the next few years.

A further important motivation for considering clusters is that they can sample the cosmic velocity field up to distances larger than those presently accessible by galaxies. On these larger scales, fluctuations are largely in the linear regime and are, therefore, more closely related to the "initial conditions" from which large–scale structure developed. In addition, since large–scale velocities are mostly sensitive to long–wavelength density fluctuations, one expects that, for a fixed choice of the fundamental cosmological parameters (Hubble constant H_0, density parameter Ω_0 and cosmological constant term Ω_Λ), the amplitude of large–scale motions is almost independent of the composition of the dark matter (DM) component (i.e., cold vs. hot DM). For these reasons, several authors (e.g., Bahcall, Cen & Gramann 1994; Croft & Efstathiou 1994; Bahcall, Gramann & Cen 1994; Cen, Bahcall & Gramann 1994; Strauss et

al. 1995; Gramann et al. 1995) have recently addressed the issue of whether cluster motions can be used to constrain cosmological models. Various statistical tests have been used for this purpose, among which the velocity frequency distribution, bulk flows, velocity dispersions, pairwise velocities and the velocity correlation function feature prominently.

The present work is devoted to a quantitative comparison between presently available observational data on cluster peculiar velocities and an extended set of numerical simulations of a number of different cosmological models. The simulations are based on an optimized version of the Zel'dovich approximation (Zel'dovich 1970; Shandarin & Zel'dovich 1989; Coles, Melott & Shandarin 1993), the ability of which to simulate the large–scale distribution of galaxy clusters has been assessed by Borgani et al. (1995; see also Plionis et al. 1995). We will show in the following that the quasi–linear description of the large–scale velocity field provided by our simulation method reproduces to a good accuracy that obtained from N–body simulations. At the same time, the method is so cheap, computationally speaking, that it enables us to consider easily a large number of realizations of a large number of different scenarios.

In this paper we consider $\Omega_0 < 1$ CDM models both with and without a cosmological constant term Λ imposing the condition of spatial flatness: $\Omega_\Lambda = \Lambda/(3H_0^2)$. We also consider, as reference models, the $\Omega_0 = 1$ CDM and CHDM scenarios. Our main aim here is to investigate whether the cluster velocity field can constrain the values of Ω_0 and Ω_Λ. (In fact, for a fixed spectrum normalization, the resulting motions essentially depend on the value of Ω_0: the larger the density parameter, the larger are the peculiar velocities.)

Observational motivations for cosmological scenarios with $\Omega_0 < 1$ have been considered by different authors (cf. Coles & Ellis 1994; see Ratra & Peebles 1995 for a summary; see, however, Primack 1995, for a different view about a low–Ω_0 Universe). Due to the fact that "ordinary" inflation models can accommodate open universes only by fine tuning either the duration of inflation or the pre-inflationary conditions (e.g. Lucchin & Matarrese 1985; Ellis, Lyth & Mijic 1991), interest, in the past, has been limited only to models in which $\Omega_\Lambda \neq 0$ (Efstathiou, Sutherland & Maddox 1990; Kofman, Gnedin & Bahcall 1993). Only very recently has it been realized that, in the framework of the bubble nucleation model, it is possible to obtain an open geometry, regardless of the initial conditions, but requiring only an appropriate choice for the scalar field potential (Sasaki et al. 1993; Bucher, Goldhaber & Turok 1995); see Linde & Mezhlumian (1995), and references therein, for a review of this class of inflationary models. An extensive comparison of the predictions of open CDM models with a variety of observational data is given by Liddle et al. (1995) and Yamamoto & Bunn (1995); see also Ratra & Peebles (1994).

The layout of this paper is as follows. In Section 2 we present our approach for simulating the cluster velocity field and we discuss its reliability by comparing relevant results with those obtained using an N–body code. We also describe the statistical tests applied in the analysis and briefly introduce the suite of cosmological models we consider. In Section 3 we compare the output for different initial spectra in terms of both the velocity frequency distribution and the velocity correlation function. Section 4 is devoted to a comparison with available observational data; in particular we study the bulk flow and the cumulative velocity frequency distribution. In Section 5 we discuss our results and, finally, we draw our main conclusions in Section 6.

2 THE SIMULATIONS

2.1 The Zel'dovich approach

Our simulations mimic gravitational dynamics through the Zel'dovich approximation (ZA; Zel'dovich 1970; Shandarin & Zel'dovich 1989). This method is based on the Eulerian–to–Lagrangian space mapping

$$\mathbf{x}(\mathbf{q},t) \, = \, \mathbf{q} - b(t)\nabla\psi(\mathbf{q}) \, , \qquad (1)$$

where $\mathbf{q}$ and $\mathbf{x}$ are initial and final particle positions, respectively, $b(t)$ is the fluctuation linear growth factor and the velocity potential $\psi(\mathbf{q})$ is related to the initial fluctuation field by the Poisson equation. The simulation procedure has been described in detail in Borgani et al. (1995; hereafter Paper I), to which we refer the reader for more details. Here we simply recall that the initial power spectrum is convolved with a Gaussian window, $P(k) \rightarrow P(k)e^{-k^2R_f^2}$, in order to suppress shell–crossing at small scales (Coles, Melott & Shandarin 1993; Melott, Pellman & Shandarin 1994). The filtering radius R_f is chosen in such a way that the average number of streams at each Eulerian point (Kofman et al. 1994) is $N_s = 1.1$. After assigning the linear potential on a grid, particles are moved from their initial grid positions according to eq.(1). The density

and potential fields are then reassigned on the grid and clusters are selected as the highest local density maxima, so as to reproduce the observed Abell/ACO cluster number density, $n_{cl} \simeq 1.8 \times 10^{-5} (\, h^{-1}\mathrm{Mpc})^{-3}$, which corresponds to $d_{cl} \simeq 38\, h^{-1}\mathrm{Mpc}$ for the mean cluster separation. The parameter h is the Hubble constant in units of $100\,\mathrm{km\,s^{-1}\ Mpc^{-1}}$.

Velocities at the grid positions are evaluated by following two different prescriptions.

(a) Defining the particle velocities as $\mathbf{v} \propto -\nabla\psi(\mathbf{q})$ and interpolating their mass and momentum on the grid with the TSC scheme (Hockney & Eastwood 1981). The velocity at the grid point is then defined as the ratio between the local values of momentum and mass (e.g., Kofman et al. 1994). This linear prescription, that we will name LIN in the following, amounts to the assumption that particles at the final positions do not still feel any tidal force and move according to the initial (*linear*) gravitational potential.

(b) Computing the gradient of the ZA–evolved potential, ψ_{ZA}, which is connected by the Poisson equation to the density fluctuations, δ_{ZA}, traced by the final particle distribution, $\nabla^2\psi_{ZA} = 4\pi G\bar{\rho}a^2\delta_{ZA}$. Accordingly, $\mathbf{v} \propto -\nabla\psi_{ZA}$. In this quasi–linear prescription, named ZEL in the following, one assumes that, although the density field has undergone a substantial non–linear evolution, it is still connected to the velocity by a linear relationship.

Non–linear effects in the velocity field, such as infall and merging, are not accounted for in this simulation method. These effects, however, are only expected to dominate on scales $\lesssim$ 10–20 h^{-1}Mpc, where the observational data on cluster peculiar velocities are in any case rather unreliable.

2.2 Comparison with N–body velocities

In Paper I we noted that, while the ZA is very accurate at locating clusters in the correct positions for models with $\sigma_8 \lesssim 1$ [σ_8 is the rms fluctuation amplitude within a top–hat sphere of radius $8\, h^{-1}$Mpc radius], non–linear gravitational effects on the cluster mass scale degrade this precision when $\sigma_8 \gtrsim 1$. However, this is not expected to represent a limitation for the present analysis. In fact, in order to study the cluster velocity field it is not necessary to know cluster positions with any great precision. What we need from simulations is only a population of objects tracing the large–scale flows having the same sampling density and same selection biases as real clusters do.

Before presenting the results of our analyses, it is important to assess the reliability of our approach to the simulation of the cluster velocity field. We therefore begin by comparing results of our approach with those obtained from the same N–body simulation we previously used in Paper I for the comparison of cluster positions. The initial spectrum corresponds to the Cold+Hot DM (CHDM) model with 30% of hot component (see next section). The box size is $320\, h^{-1}$Mpc (with $h = 0.5$) and the number of grid points and particles is 128^3. We do not distinguish between hot and cold particles, since any effect of residual free-streaming should be negligible at the smallest scales $r \gtrsim 2.5\, h^{-1}$Mpc allowed by our resolution.

In the N–body simulation clusters, are identified as local maxima on the grid, following the same method outlined in the previous subsection. The velocity at the grid point positions is defined by following prescription **(a)**, previously described, with the difference that non–linear (final) particle velocities are now used and that density and momentum are smoothed with a top–hat filter of width $10\, h^{-1}$Mpc to create continuous fields and to ensure that the density is non–zero at each grid point.

For comparison we run a ZA simulation having the same initial spectrum and random phase assignment and assuming the same box size and resolution. We show results at two different evolutionary stages, corresponding to $\sigma_8 = 0.67$ and $\sigma_8 = 1$. Even though the two–year *COBE* data (Bennett et al. 1994) are roughly consistent only with the first epoch, we consider the second, higher, normalization as well, in order to assess the reliability of the ZA approach in a more evolved situation, when the cluster mass scale starts to become non–linear. The filtering radii, R_f, applied in the ZA simulation are $R_f = 2.3$ and $R_f = 4.5\, h^{-1}$Mpc for $\sigma_8 = 0.67$ and $\sigma_8 = 1$, respectively. In the following we will compare the velocity fields traced by the clusters identified in the N–body simulation and in the ZA simulation, by adopting the two definitions (LIN and ZEL) of velocity described above.

2.2.1 General features of the velocity fields

In Figure 1 we compare the velocity fields traced by clusters within a slice $60\, h^{-1}$Mpc thick for the PM and ZA simulations. The fields are recovered by smoothing the velocities associated to the PM and ZA cluster positions with a Gaussian window of radius $20\, h^{-1}$Mpc.

The resulting velocity field is then reassigned on 16^3 grid points. All clusters are equally weighted, independently of their masses. At the first stage ($\sigma_8 = 0.67$), there is a strong correspondence between the cluster velocity fields obtained by different methods: all the main features are well reproduced at the correct locations. At $\sigma_8 = 1$, although the principal stream lines are still well delineated, there is a slight tendency for both ZEL and LIN to overestimate the velocity amplitude.

It is quite interesting to follow the evolution of the non–linear feature at the centre of the panels displayed, where some degree of infall (convergence of stream lines) takes place. At $\sigma_8 = 0.67$ this feature is quite well reproduced by the LIN and ZEL velocities. However, at $\sigma_8 = 1$ the higher degree of infall displayed by the N–body velocities is not reproduced by the LIN and ZEL fields. As the degree of non–linearity increases, shell–crossing becomes more and more important: stream lines consequently cross each other, instead of simply converging towards potential minima.

2.2.2 Statistical tests

In order to obtain a more quantitative assessment of the reliability of our approach, we analyze PM, LIN and ZEL velocity fields with the same statistical tests to be applied in the analysis of the data we perform later. They are the 3D velocity frequency distribution (VFD), the velocity correlation function and the bulk flow (as a function of scale). Figure 2 summarizes the results at the two evolutionary stages.

The VFD $P(v)$ is defined as the fraction of cluster velocities in a given range. The results of $P(v)$ for the 3D cluster velocity field are shown in the upper panels. We used a Kolmogorov–Smirnov (KS) test to compute the significance level for the null hypothesis that the different VFDs are drawn from the same distribution. Comparing LIN to ZEL and PM, we find significant departures at both output times: the distribution peak for LIN is always shifted to lower velocities ($\sim$ 300 versus $\sim 450 - 500\,\mathrm{km\,s^{-1}}$ at $\sigma_8 = 0.67$ and $\sim$ 500 versus $\sim 600 - 650\,\mathrm{km\,s^{-1}}$ at $\sigma_8 = 1$). On the other hand, the results for PM and ZEL are in good agreement: the KS test indicates high probabilities both for both $\sigma_8 = 0.67$ and $\sigma_8 = 1$.

Note that the VFD statistics do not take into account the spatial distribution of clusters; at the more evolved epoch the agreement of cluster positions between PM and ZEL is not as good (see the discussion in Paper I). In order to take into account the cluster positions in the statistics of the velocity field, we will use the velocity correlation tensor, defined as

$$\Psi_{ij}(\mathbf{r}) \equiv \langle v_i(\mathbf{r_1}) v_j(\mathbf{r_2}) \rangle. \tag{2}$$

Here, $\mathbf{r_1}$ and $\mathbf{r_2} = \mathbf{r_1} + \mathbf{r}$ are the position vectors of two objects having peculiar velocities $\mathbf{v}(\mathbf{r_1})$ and $\mathbf{v}(\mathbf{r_2})$, respectively (Górski 1988; Górski et al. 1989). In general what one estimates is the scalar velocity correlation function $\xi_v(r)$ which is defined as the trace of the velocity correlation tensor, $\xi_v = |\sum_i \Psi_{ii}|^{1/2}$. According to its definition, $\xi(v)$ is a measure of the coherence of the velocity field: if at some scale a coherent bulk flow dominates the velocity field, ξ_v will be positive; infall or outflow velocities result in a negative contribution to ξ_v.

The velocity correlation function $\xi_v(r)$ is plotted in the central panels of Figure 2. Error bars, shown only for the PM results, are 1σ uncertainties computed using the bootstrap technique. The agreement between different determinations is good at both epochs: only at very small distances ($r \lesssim 20\,h^{-1}\mathrm{Mpc}$), some differences (always smaller than 2σ) are present.

The last test we consider is the bulk velocity V_{bulk}, defined as the centre–of–mass velocity of a specified region and given by the integral of the peculiar velocities $\mathbf{v}(\mathbf{x})$ over a selected volume specified by a selection function $\phi(\mathbf{x})$:

$$\mathbf{V}_{\mathrm{bulk}}(r) = \int_0^r \phi(\mathbf{x})\, \mathbf{v}(\mathbf{x})\, \mathrm{d}\mathbf{x}. \tag{3}$$

In our case the velocity field is traced by galaxy clusters and eq.(3) becomes

$$\mathbf{V}_{\mathrm{bulk}} = \sum_i w_i \mathbf{v}_i / \sum_i w_i, \tag{4}$$

where i refers to different clusters inside the considered region. The weights w_i account for cluster masses, inhomogeneous sampling and uncertainties in the cluster positions. The choice of the weighting scheme is particularly important when one deals with observational biases, and several different schemes have been proposed in literature. For the purpose of this analysis, we are studying a perfectly sampled cluster distribution, for which the cluster masses and peculiar velocities are known, so the natural weighting scheme to implement is simple number weighting (i.e. $w_i = 1$).

Results for the bulk velocity statistics are shown in the lower panels of Figure 2. Also in this case we plot the error bars only for the N–body results: they are obtained as standard deviation of bulk flows computed for 10,000 different observers. Note that the rather small

box size is expected to result in a significant underestimate of $V_{\rm bulk}$ at scales $\gtrsim$ 70–100 h^{-1}Mpc. However, here we are interested only in a relative comparison of the different simulation methods rather than estimating the absolute value of the different model bulk flows. At $\sigma_8 = 0.67$, ZEL simulations provide a reliable estimate of $V_{\rm bulk}$ on scales larger than $20\,h^{-1}$Mpc. The situation is even better at $\sigma_8 = 1$: here the agreement between PM and ZEL is well inside the 1σ range at all scales. On the other hand, the LIN simulation tends to underestimate the bulk flow at small scales when $\sigma_8 = 1$.

We conclude from this analysis that the quasi–linear definition ZEL gives a good representation of the velocity field traced by clusters over the whole scale range, even at the stage $\sigma_8 = 1$, when substantial non–linearity appears on the cluster mass scale. This is particularly relevant for those statistics incorporating both position and velocity information, such as the velocity correlation function and bulk flow. We will therefore use the ZEL velocity definition in our cluster simulations from now on.

2.3 Models for the power spectrum

As we have explained, our aim is to use the cluster velocity field to constrain the value of the density parameter Ω_0, both with and without a cosmological constant term, Ω_Λ, assuming the context of a CDM scenario. We considered values of the density parameters corresponding to $\Omega_0 = 0.2, 0.3, 0.4, 0.6, 0.8$. In addition, we also simulated two $\Omega_0 = 1$ models, namely the standard CDM model (SCDM) and a Cold+Hot DM (CHDM) model with 30% of hot component. We therefore end up with 12 models for the forthcoming analysis. They are listed in Table 1, in which OCDM stands for the open models and ΛCDM for the models with a non–zero cosmological constant term.

For the CDM power spectra we assumed the expression provided by Efstathiou, Bond & White (1992), with the shape parameter $\Gamma = \Omega_0 h \exp(-\Omega_B - \Omega_B/\Omega_0)$, corrected according to the prescription of Peacock & Dodds (1994) to account for the presence of baryons (Sugiyama 1995). We take the density parameter in baryons to be $\Omega_B = 0.013h^2$, as suggested by standard nucleosynthesis (e.g. Reeves 1994). The transfer function provided by Holtzman (1989) is used for the CHDM spectrum. For each pair of $(\Omega_0, \Omega_\Lambda)$ values, we choose the Hubble parameter h in such a way that the age of the universe

$$t_0 = H_0^{-1} \int_1^\infty \frac{dx}{x\sqrt{\Omega_0 x^3 + (1-\Omega_0-\Omega_\Lambda)x^2 + \Omega_\Lambda}} \quad (5)$$

(see, e.g., Peebles 1993) is $t_0 \simeq 12$ Gyr for all the models, except for SCDM and CHDM, for which we assume $h = 0.5$, giving $t_0 \simeq 13$ Gyrs. Although $t_0 \simeq 12$ Gyrs seems to be slightly too small in comparison to most current estimates of the age of the universe (e.g. Chaboyer et al. 1995; arguments in favour of $t_0 \simeq 11$ Gyrs from globular cluster ages have also been advanced, e.g., Shi 1995), we adopt this value of t_0 for the low–Ω_0 models so as to obtain almost the same age as with the usual choice of $h = 0.5$ for the $\Omega_0 = 1$ models.

To normalize the two $\Omega_0 = 1$ models to COBE, we use $Q_{rms-PS} = 20\mu K$ (Górski et al. 1994). In the case of the OCDM models, we resort to the normalization procedure outlined by Górski et al. (1995). The procedure is straightforward to implement, since we select models with the same criteria as Górski et al. (1995) did in their Table 1. We take for σ_8 the central value in their reported 1σ range, which is associated to uncertainties in the Q_{rms-PS} estimates.

For the ΛCDM models, Efstathiou et al. (1992) proposed the relation

$$Q_{rms-PS} = \left(\frac{5}{6\pi^2}\right)^{0.5} \left(\frac{H_0}{2c}\right)^2 T_0 \Omega_0^{0.77} B^{0.5}\,, \quad (6)$$

($T_0 = 2.735$ K) which connects the purely Sachs–Wolfe (SW) quadrupole to the amplitude B of the primordial power spectrum, $P(k) = Bk$. However, as, for example Stompor, Górski & Banday (1995; hereafter SGB) have pointed out, significant additional contributions to the radiation power spectrum come from the integrated SW effect induced by the cosmological constant. Unfortunately, these authors reported, in their Table 2, the σ_8 normalizations only for models with two fixed values of h, namely $h = 0.5$ and $h = 0.8$. In order to fix the normalization for the models corresponding to different choices of h, we proceed as follows. SGB noted that the integrated SW effect is negligible for $\Omega_0 \gtrsim 0.5$. Therefore, we use for $\Omega_0 \geq 0.5$ the pure SW normalization provided by eq.(6). On the other hand, from Figure 3 of SGB, it turns out that for our $\Omega_0 < 0.5$ models the σ_8 normalization essentially depends on the value of $\Omega_0 h^2$. Therefore, we compute the $\Omega_0 h^2$ value for each model and use this plot to normalize our spectra when $\Omega_0 < 0.5$. We expect the accuracy of this procedure to be within 10%–15%, of the same order of the statistical and systematic deviations estimated by SGB in their analysis.

The values of σ_8 for all the considered models are shown in Table 1, where we also report the filtering radii R_f used to suppress shell–crossing in the ZA (see Section 2.1).

[tp]

Table 1. The model parameters. Column 2: the density parameter Ω_0; Column 3: the cosmological constant term Ω_Λ; Column 4: the Hubble parameter h; Column 5: the linear rms fluctuation amplitude at $8\,h^{-1}$Mpc σ_8; Column 6: the filtering radius R_f (in h^{-1}Mpc).

Model	Ω_0	Ω_Λ	h	σ_8	R_f
SCDM	1.0	0.0	0.50	1.36	6.0
CHDM	1.0	0.0	0.50	0.78	3.3
OCDM02	0.2	0.0	0.70	0.31	0.5
OCDM03	0.3	0.0	0.65	0.50	1.6
OCDM04	0.4	0.0	0.65	0.75	3.1
OCDM06	0.6	0.0	0.60	1.10	4.9
OCDM08	0.8	0.0	0.55	1.30	5.8
ΛCDM02	0.2	0.8	0.87	1.20	5.8
ΛCDM03	0.3	0.7	0.78	1.44	6.9
ΛCDM04	0.4	0.6	0.72	1.54	7.2
ΛCDM06	0.6	0.4	0.64	1.47	6.6
ΛCDM08	0.8	0.2	0.58	1.43	6.3

For each model we ran a single realization within a box of $960\,h^{-1}$Mpc on a side, using 256^3 grid points and particles. With the adopted cluster mean separation, we end up with about 16,000 objects in each simulation box. The very large size of the box ensures that: *(a)* no appreciable box–to–box variance is present in the final results (we verified this by running two realizations for ΛCDM02 and CHDM models); *(b)* fluctuation modes with wavelengths larger than the box size make a negligible contribution to bulk flows and velocity correlations. Indeed, our analysis is confined within $180\,h^{-1}$Mpc, which is roughly the scale where the reconstructed bulk flow traced by Abell/ACO clusters is reliable (Branchini, Plionis & Sciama 1995; BPS hereafter).

3 COMPARISON BETWEEN MODELS

In this section we consider the 3D velocity frequency distribution and the velocity correlation function, with the aim of quantifying intrinsic differences between models. Any comparison with observational data and how observational uncertainties are taken into account in simulation analysis will be discussed in the next section.

3.1 The velocity frequency distribution

As a first test, we consider the VFD $P(v)$ for the 3D cluster velocity field. We compute the VFD for the whole box for each of the simulations. In Figure 3 we plot the results for SCDM and CHDM models (top left panel), the OCDM models (top right panel) and ΛCDM models (bottom left panel). As expected, models with low Ω_0 generate smaller velocities, independently of the presence of the cosmological constant. However, the Ω_Λ term tends to increase the average peculiar velocity and is also effective in concealing differences in the VFDs among various Ω_0 choices. Consequently, ΛCDM models have VFDs that are similar to each other for $\Omega_0 \geq 0.4$, while the analogous OCDM models show much better separated VFD curves. The model with the largest velocities is SCDM while the probability of having very large velocity in CHDM is smaller than in several of the low density models.

Due to their small size, we prefer not to plot the error bars, estimated as scatter between the two realizations of CHDM and ΛCDM02 models. Their smallness is a consequence of the large dimension of the simulation box and confirms that the box size we adopted is large enough to avoid any significant effect of cosmic variance. This is especially true for CHDM, which has a smaller relative amount of large–scale power and, consistently, displays a smaller dispersion than ΛCDM02. Therefore, we expect that uncertainties in the analysis of realistic simulated samples (see next section) will be associated with the limited number of included clusters and to the observer–to–observer scatter, rather than to the cosmic variance arising from the finite box size.

Considering N–body simulations of different cosmological scenarios (SCDM, ΛCDM03 and $\Omega_0 = 0.3$ primeval baryonic isocurvature models), Bahcall, Cen & Gramann (1994) showed that the shape of the cluster velocity distribution is well matched by a Maxwellian distribution $P(v) \propto v^2 \exp(-v^2/2\sigma_v^2)$, where σ_v is the velocity dispersion. This result is expected when a Gaussian distribution for the initial density fluctuations is assumed and effects of non–linear gravitational clustering are negligible at determining cluster velocities. Using the value of σ_v obtained from the VFDs of our simulations, we found that a Maxwellian distribution provides a good representation for all considered models. In Figure 3 the fitting curves are plotted (dashed lines) for clarity only for the two $\Omega_0 = 1$ models: they are almost indistinguishable from the simulated data and closely resemble the result of Bahcall et al. (1994a), which is based on N–body experiments.

3.2 The velocity correlation function

Cen, Bahcall & Gramann (1994) showed that the velocity correlation function $\xi_v(r)$, especially at small separation, is strongly dependent on cosmological models, and therefore represents a potentially useful tool for constraining them. However, with the observational data currently available it is very difficult to obtain a determination of the cluster velocity correlation function, which is sufficiently reliable to be effectively compared it with simulated data, although Croft & Efstathiou (1995) have recently succeeded in applying a maximum likelihood analysis to the velocity correlations estimated from two sets of observational data, finding marginal evidence for more power than the standard CDM model.

In Figure 4 we plot $\xi_v(r)$ for the considered models at scales $r \geq 20\,h^{-1}$Mpc, where the ZA description of the velocity correlations has been shown to be reliable. Consistent with the results from the VFD analysis, OCDM models are characterized by a progressively larger $\xi_v(r)$ as Ω_0 increases. A clear discrimination between models is possible up to scales $r \simeq 60\,h^{-1}$Mpc, while above $100\,h^{-1}$Mpc all the models seem to converge, with the exception of OCDM02. Among the ΛCDM models, the only one with a significantly different behaviour is ΛCDM02: all the other spectra provide almost indistinguishable velocity correlations.

We note also that the velocity correlation functions of different realizations for CHDM and ΛCDM02 models are extremely similar, thus indicating that cosmic variance is negligible in such big simulation boxes.

4 COMPARING MODELS AND OBSERVATIONS

In this section we attempt to constrain the different cosmological models by comparing predictions of properties of the cluster peculiar velocity field with relevant available data. To this end, we compute both the bulk flow and the cumulative velocity frequency distribution. We prefer not to consider velocity correlations, since estimating ξ_v in a meaningful way would require a large, statistically complete sample of accurate cluster peculiar velocities, which is not available at present.

4.1 Cluster velocity data

Unlike the simulation case, estimating the bulk flow executed by real clusters is a non–trivial task, since the available cluster IRTF and D_n–σ peculiar velocity data are sparse and inhomogeneous. Furthermore, only the line–of–sight component of the peculiar velocity is observed. These limitations can significantly affect the determination of the observational bulk velocity (Kaiser 1988; Regös & Szalay 1989) and they have to be taken properly into account if one wants to compare observational and model bulk flows. Therefore, in the following, we will use the IRTF and D_n–σ cluster peculiar velocities to compute only the cumulative velocity frequency distribution (CVFD), $P(> v)$, i.e. the fraction of clusters with a velocity greater than v (the VFD is its differential version) and compare it with model predictions.

A possible way to avoid the above–mentioned problems in the context of the bulk flow test is to reconstruct the full 3D cluster peculiar velocity field from their observed redshift space distribution [see Dekel (1994) and Strauss & Willick (1995) for reviews of the reconstruction methods available]. In the following analysis we will consider the bulk velocity derived from the reconstructed Abell/ACO cluster density field of Branchini & Plionis (1995) and Branchini et al. (1995), hereafter BPS. These authors found a good consistency between their bulk flow and their derived 3D smoothed density field, and independent measurements contained within a depth of 8000 km s^{-1} in the Mark III galaxy sample (cf. Dekel 1994; Hudson et al. 1995). We will also use the BPS velocities to constrain model predictions of $P(> v)$.

4.1.1 Observational velocities

We construct our composite observational catalogue from cluster peculiar velocity determinations by Aaronson et al. (1986), Mould et al. (1991,1993), Han & Mould (1992) and Mathewson, Ford & Buchhorn (1992), which are all based on IRTF measurements. We add the further data reported in Table 7 by Mould et al. (1991), which contains peculiar velocities obtained both with the IRTF method (Aaronson et al. 1989) and with the D_n–σ technique (Lucey & Carter 1988; Faber et al. 1989). Finally, we include cluster velocities obtained by Hudson (1994), both with D_n–σ and IRTF techniques, and the recent IRTF data from Giovanelli (1995; see also Giovanelli et al. 1995). Of course, it is possible that more than one velocity determination is available for any given cluster: in such cases we have chosen to include in the catalogue only the determination with the smallest error. The result of this selection is an interim sample of 65 objects, with a very inhomogeneous spatial distribution. Some of these clusters show very large

[tp]

Table 2. The composite catalogue of observed cluster peculiar velocities. Column 1: the source of the data; Column 2: the method used; Column 3: the number of cluster peculiar velocities available in the original paper; Column 4: the number of objects actually used in the composite catalogue.

Source	Method	Available	Used
Aaronson et al. (1986)	IRTF	10	0
Mould et al. (1991) [a]	IRTF	9	6
Mould et al. (1991) [b]	IRTF	16	1
Mould et al. (1991) [c]	D_n–σ	16	1
Han & Mould (1992)	IRTF	21	6
Mathewson et al. (1992)	IRTF	24	10
Mould et al. (1993)	IRTF	8	8
Hudson (1994)	IRTF	21	1
Hudson (1994)	D_n–σ	17	6
Giovanelli (1995)	IRTF	23	23
TOTAL			62

[a] from Table 6.
[b] from Table 7 (Aaronson et al. 1989).
[c] from Table 7 (Lucey & Carter 1988; Faber et al. 1989).

errors and we prefer to exclude them from our analysis to obtain a more robust result. We therefore decided to consider only objects with peculiar velocity uncertainties smaller than 850 km s^{-1}, excluding 2 objects, namely 2159–32 from Mathewson et al. (1992) and Hercules from Aaronson et al. (1986). We have verified that our conclusions do not change if we exclude the clusters with velocity errors larger than 450 km s^{-1}, so as to end up with a smaller catalogue of 43 objects. Finally, we also reject the data of Cen45, whose determination is uncertain and controversial, with different authors reporting greatly discrepant results [i.e. 203 ± 383 km s^{-1} from Han & Mould (1983), while 1663 ± 336 km s^{-1} from Mould et al. (1991); note that both results are obtained with the IRTF method]. At the end, the composite sample contains 62 objects, whose sources are detailed in Table 2.

Due to the two different methods used (IRTF and D_n–σ relations) and to the absence of an inner calibration of the data coming from different sources, our composite sample may be affected by some basically uncontrollable biases. For these reasons, after discussing results coming from the composite sample, we will also present results obtained using data coming from unique sources.

4.1.2 BPS *reconstructed velocities*

Branchini et al. (1995) adopt a two step procedure to recover the real–space positions and peculiar velocities of Abell/ACO clusters, within $cz \leq 25,000$ km s^{-1}, starting from their redshift space positions.

- As a first step, BPS generate, via Monte Carlo techniques, several different realizations of a synthetic cluster population, spatially correlated with the observed clusters, so as to correct for selection effects and properly homogenize the Abell and ACO catalogues. The outcome is an all–sky volume limited distribution of synthetic + real clusters in redshift space.
- The second step is the application of an iterative technique, similar to that proposed by Strauss & Davis (1988) and Yahil et al. (1991), which assumes linear theory and linear biasing, to reconstruct the true cluster positions from their observed redshifts.

The velocity of each cluster is, thus, essentially obtained from its measured dipole evaluated at its reconstructed real space position. Taking into account the uncertainties due to the intrinsic error of their method as well as the uncertainties related to modelling the observational parameters (galactic absorption, Abell/ACO homogenization procedure, etc.), BPS estimated their mean cluster velocity error to be ≈ 170 km s^{-1} with a dispersion of about 90 km s^{-1} around this value.

We note that the BPS reconstruction method is based on two assumptions, namely that: **(a)** linear gravitational instability holds and **(b)** the simple linear biasing relation, $\delta n/n = b(\delta\rho/\rho)$, connects fluctuations in cluster number counts and DM density, with a position–independent biasing parameter b. While the former assumption is expected to be satisfied at the large scales relevant in our analysis, the latter is probably an oversimplification. Although its effect, in the light of the success of the reconstruction method (cf. BPS), is likely not to be dramatic it could nevertheless introduce uncertainties into the individual cluster velocities which are not included in the previous quoted errors.

We will use the 280 clusters within $cz \leq 20,000$ km s^{-1}, since BPS consider their cluster velocity field to be reliable out to to this depth. Beyond $cz = 20,000$ km s^{-1} the redshift selection function drops exponentially while for $cz > 25,000$ km s^{-1} they have used the rather crude assumption of a homogeneous universe in their reconstruction algorithm.

4.2 The Bulk Flow Analysis

In order to perform a consistent comparison between simulations and real data, one would desire in principle to reproduce the observational set–up as closely as possible. We place observers at grid points and define their local density contrast $\delta_{\rm obs}$ and bulk velocity averaged over a top–hat sphere of radius $R = 7.5\,h^{-1}$Mpc centred on them. The local value of $\delta_{\rm obs}$ is estimated by convolving the Fourier transform of the fluctuation density field with the Fourier transform of the top–hat window, $W(kR) = 3(\sin kR - kR\cos kR)/(kR)^3$. The observer's velocity is defined using the same procedure adopted for the cluster velocity. We estimate $\delta_{\rm obs}$ and the peculiar velocity for 80,000 observers chosen at random grid positions in each simulation. We then select those 'observers' that have the same characteristics as the Local Group, the number of which is also considered as a test for DM models (Górski et al. 1989; Tormen et al. 1993; Strauss et al. 1995; Moscardini et al. 1995; Tini Brunozzi et al. 1995). These characteristics are:

(1) peculiar velocity $V_{\rm LG} = 627 \pm 44\,{\rm km\,s^{-1}}$ (error corresponding to 2σ uncertainties; Kogut et al. 1993) for a top–hat sphere of radius $R = 7.5\,h^{-1}$Mpc centred on the observer;
(2) density contrast within the same sphere in the range $-0.2 \leq \delta_{LG} \leq 1$.

We decided to neglect in this analysis a further requirement concerning the quietness of the local flow, which implies a small value for the local shear. In fact, we expect that any shear is poorly represented by the velocity description provided by our simulations. In any case, as shown by Moscardini et al. (1995), the local shear constraint is not a particularly restrictive one.

In Column 2 of Table 3 we report the fractions $\mathcal{F}_{LG}$ of observers satisfying the LG requirements. The results for different models are quite similar, with the highest probability occurring for OCDM06 and ΛCDM03 models. The only exceptions are represented by the open models with $\Omega_0 \leq 0.3$, where none of the chosen grid points has the desired characteristics. This problem for the open models with very low Ω_0 and small σ_8 was already noted in Tormen et al. (1993). Due to the impossibility of defining LG observers in these cases, we prefer to consider in the following analysis 2000 observers randomly chosen in the list of 80,000, dropping completely the LG constraints. We checked that, at least for those models having a large enough number of LG–like observers, this choice does not affect the results significantly.

A self–consistent comparison with the BPS bulk velocity would, strictly speaking, require us to apply their method also on the simulated cluster distribution, starting from their redshift–space positions. We have performed such a test on a subset of CHDM and ΛCDM observers and we found a very good agreement between the profiles of the "true" and reconstructed bulk flows. On the other hand, their amplitude can be matched a posteriori, by an appropriate choice of the (observer–averaged) cluster biasing parameter b (we note that such definition of b does not necessarily coincide with that based on the ratio of rms fluctuations in cluster counts and DM density; but see Kolokotronis et al. 1995). Having assessed the agreement between "true" and reconstructued bulk flows, we decided to compare the BPS data to the original ZEL cluster velocities, since applying the reconstruction procedure for all the 2000 observers selected in each model would require a very time–consuming computation.

The cluster bulk velocity for the simulations was computed as follows: for each selected observer we measure the bulk velocity in spheres of increasing radius using eq.(4) with $w_i = 1$ (we verified that very similar results are obtained using a mass weighing scheme, i.e. with $w_i \propto m_i$, where m_i is the cluster mass). Due to the large intercluster separation, we started measuring the bulk velocity within spheres of radius $50\,h^{-1}$Mpc to have reliable estimates. A limiting depth of $180\,h^{-1}$Mpc has been chosen to allow a meaningful comparison with the BPS data.

The scale–dependence of the bulk flow averaged over the 2000 observers is plotted in Figure 5 for all the cosmological models we have considered. The shaded region represents the 1σ strip allowed by the BPS data. A simple visual analysis reveals that the only models we can rule out at a level larger than 1σ are the OCDM ones with $\Omega_0 < 0.4$. Flat models with non–vanishing cosmological constant, as well as CHDM and SCDM are in good agreement with the data on scales larger than $\simeq 100\,h^{-1}$Mpc. On smaller scales only the CHDM model is well inside the observational strip. As a more quantitative analysis, we estimate, for each model, the fraction of observers whose measured bulk flow has certain specific properties. The corresponding probabilities are also reported in Table 3. In Column 3 we list the fraction of observers $\mathcal{F}_{50}$ measuring a bulk flow at $50\,h^{-1}$Mpc within 1σ from the BPS value. We choose

[tp]

Table 3. The fractions of observers measuring a particular characteristic in different cosmological models. Column 2: satisfying the Local Group requirements (see text; $\mathcal{F}_{LG}$); Column 3: bulk flow within 1σ from the Branchini et al. (1995) value at $50\,h^{-1}$Mpc ($\mathcal{F}_{50}$); Column 4: bulk flow within 1σ from the Branchini et al. (1995) value at $150\,h^{-1}$Mpc ($\mathcal{F}_{150}$); Column 5: bulk flow within 1σ from the Lauer & Postman (1994) value at $\sim 100\,h^{-1}$Mpc ($\mathcal{F}_{LP}$); Column 6: bulk flow within 2σ from the Branchini et al. (1995) values in the range from 50 to $150\,h^{-1}$Mpc ($\mathcal{F}^{2\sigma}_{all}$).

Model	$\mathcal{F}_{LG}$	$\mathcal{F}_{50}$	$\mathcal{F}_{150}$	$\mathcal{F}_{LP}$	$\mathcal{F}^{2\sigma}_{all}$
SCDM	0.026	0.293	0.365	0.032	0.109
CHDM	0.053	0.437	0.315	0.019	0.237
OCDM02	$< 10^{-3}$	0.017	$< 10^{-3}$	$< 10^{-3}$	0.019
OCDM03	$< 10^{-3}$	0.046	0.013	$< 10^{-3}$	0.094
OCDM04	0.015	0.383	0.108	$< 10^{-3}$	0.228
OCDM06	0.070	0.409	0.300	0.009	0.187
OCDM08	0.038	0.343	0.379	0.021	0.151
ΛCDM02	0.052	0.396	0.385	0.047	0.278
ΛCDM03	0.070	0.299	0.403	0.088	0.161
ΛCDM04	0.051	0.274	0.418	0.068	0.141
ΛCDM06	0.038	0.312	0.375	0.042	0.135
ΛCDM08	0.030	0.310	0.382	0.020	0.119

this depth since it is still within the range spanned by galaxy catalogues incorporating peculiar velocities. Moreover, at $50\,h^{-1}$Mpc the BPS bulk velocity overlaps with that obtained from the POTENT analysis (Dekel 1994) and with that measured using the recent da Costa et al. (1995) data. Similarly, Column 4 contains the probability measured at $150\,h^{-1}$Mpc ($\mathcal{F}_{150}$). Although this is also the *limiting* depth of the Lauer & Postman (1994) sample, we have compared their bulk velocity ($V_{\rm bulk} \sim 700\,{\rm km\,s^{-1}}$), which is much higher than that of BPS, at a depth of $\sim 100\,h^{-1}$Mpc which corresponds to the *effective* depth of their sample. The fraction of observers measuring a bulk flow within 1σ from the Lauer & Postman (1994) one is listed in Column 5 ($\mathcal{F}_{LP}$). Finally we measured the fraction of observers whose cumulative bulk velocity is within the 2σ strip of the BPS data throughout the range from 50 to $150\,h^{-1}$Mpc (Column 6, $\mathcal{F}^{2\sigma}_{all}$). In this case we preferred to consider a larger range (2σ) in order to have more robust statistics. The comparison with data at $50\,h^{-1}$Mpc and $150\,h^{-1}$Mpc confirms the visual impression: the only disfavoured models are the OCDM ones with $\Omega_0 = 0.2$ and 0.3 and, more marginally and only at $150\,h^{-1}$Mpc, the $\Omega_0 = 0.4$ case. Moreover, for all models the Lauer & Postman (1994) observation is a very low probability event. The same conclusion was reached using various techniques (Feldman & Watkins 1994; Tegmark, Bunn & Hu 1994; Jaffe & Kaiser 1994; Strauss et al. 1995). Finally, in the open $\Omega_0 = 0.2$ and 0.3 CDM models, a very tiny fraction of observers measures a cumulative bulk velocity in accordance with the BPS data in the whole range of scales spanned by data; the other models give similar results.

4.3 Statistics of the velocity distribution

In order to compare the data properly with the simulations, we need to take account of the (fairly large) uncertainties in cluster velocity determinations. To this end, we convolve simulated cluster velocities using the following procedure. Let v_i be the intrinsic line–of–sight velocity for the i–th model cluster ($i = 1, \ldots, 16000$) and δv_j the velocity error for the j–th randomly selected real cluster. The convolved velocity, $\tilde{v}_i$, of the model cluster is obtained by randomly generating it from a Gaussian distribution with mean v_i and dispersion δv_j. After repeating this operation for all the clusters in a simulation, we end up with a sample of error–convolved cluster peculiar velocities.

To estimate the uncertainty in the CVFD for the observational data, due to individual velocity errors, we resample the real cluster velocities as follows. For each cluster having raw velocity v and error δv, we generate a velocity v' which is randomly taken from a Gaussian distribution, having mean v and dispersion δv. A resampling of the original data set is therefore obtained by repeating this procedure for all the clusters. We generate 20,000 resamplings of the observational catalogues and for each of them we estimate the CVFD. The error is estimated as the scatter within this ensemble. The CVFD for the composite sample is plotted in Figure 6, where for comparison we show also the CVFDs obtained considering some of the single samples, namely the Hudson (1994) IRTF sample, the Hudson (1994) D_n–σ sample, the Giovanelli (1995) sample and the Branchini et al. (1995) reconstructed data (see the following subsections for more details about these samples). For sake of clarity we plot error bars, corresponding to the 2σ scatter over the observer ensemble, only for the Giovanelli (1995) and for the composite samples.

4.3.1 Results for the composite observational sample

As a first characterization of the cluster velocity field, we compute for our composite sample the rms one–dimensional velocity, $\sigma_v \equiv \langle v^2_{1D} \rangle^{1/2}$. The correspond-

ing values for the simulated catalogues are reported in Table 4, both before (Column 2) and after (Column 3) error–convolution in the manner described above. The latter have to be compared with results from the line–of–sight observational peculiar velocities, which give $\sigma_v = 725 \pm 60\,\mathrm{km\,s^{-1}}$. The errors for the convolved σ_v are estimated as the 1σ scatter over an ensemble of 20,000 samples, each containing 62 randomly selected clusters taken from the whole simulation. Note that the convolution with observational errors changes significantly the values of σ_v. This is particularly true for the models with small Ω_0 (and small peculiar motions) where a large part of the measured signal comes from the error noise. In Column 4 we report the fraction $\mathcal{F}_{\sigma_v}$ of samples measuring values of the rms velocity σ_v within the 1σ observational band. As our main result, we note that observers in OCDM models with $\Omega_0 \leq 0.4$ have a very low probability of measuring the observed σ_v, while this value becomes typical if one considers $\Omega_0 \geq 0.6$. Among the ΛCDM models, only the $\Omega_0 = 0.2$ case is rather unlikely, while all the other models are in good agreement with data. Both the $\Omega_0 = 1$ models are consistent with the available observations.

The CVFDs resulting from both real data and simulations are compared in Figure 7, where the model curves represent the mean over 20,000 samples and the observational error bars are 2σ uncertainties. Again, models with very low density are disfavoured, especially for the OCDM case: they produce too few clusters with sufficiently high velocity. Moreover, we note that, although the ΛCDM08 and SCDM models have the correct σ_v, they nevertheless appear to have a systematically smaller number of clusters with low velocities ($\lesssim 600\,\mathrm{km\,s^{-1}}$). The other models appear to lie within the 2σ observational uncertainties for the whole range of velocities considered. The discriminatory power of this test is strongly reduced by the smallness of the observational sample, as well as by the size of the uncertainties in the velocity measurements. In fact, as shown in Figure 2, this test would be efficient in constraining the different models, were it not for the convolution with the observational errors which has the effect of partially washing out differences between the model CVFDs.

In order to perform a more quantitative analysis, for each model we computed also the fraction of extracted samples for which the measured CVFD assumes a value within 1σ from the observed data. We are interested in studying the velocity distribution for values corresponding to the low–velocity tail, to the peak and to the high–velocity tail of the distribution. Therefore, we decided to consider the CVFD at three different values for the velocity, i.e. $v = 0.5\sigma_v \equiv 362.5\,\mathrm{km\,s^{-1}}$, $v = 1\sigma_v \equiv 725\,\mathrm{km\,s^{-1}}$ and $v = 2\sigma_v \equiv 1450\,\mathrm{km\,s^{-1}}$, where we have taken for σ_v the observational value; we named the corresponding fractions $\mathcal{F}_{0.5}$, $\mathcal{F}_1$ and $\mathcal{F}_2$ respectively. For our data sample we find $P(> 0.5\sigma_v) = 0.537 \pm 0.051$, $P(> 1\sigma_v) = 0.245 \pm 0.041$ and $P(> 2\sigma_v) = 0.065 \pm 0.024$. The results for the different models, also reported in Table 4, confirm our previous qualitative analysis. The CVFD at low–velocity rules out the OCDM models with $\Omega_0 \leq 0.4$, and, more marginally, ΛCDM08 and SCDM models; at high velocity the models in disagreement with the real data are the open ones with $\Omega_0 \leq 0.4$ again, and ΛCDM02.

4.3.2 Results for single observational samples

We consider now three separate samples of cluster peculiar velocities, in order to study the stability of our previous results with respect to the source and the method used to obtain the data (i.e. IRTF vs. D_n–σ). In particular we consider:

(1) The Hudson (1994) D_n–σ sample, reported in his Table 2. This is a list of 17 objects with distance smaller than 8000 km s^{-1}. Unlike the Burstein (1990) sample, from which these data originate, Coma is used as the calibrating cluster; the reported random error in the calibration of the D_n–σ relation is 3.7%. As in the previous analysis, we prefer to discard the data of Cen45 because of the large discrepancy with other determinations.

(2) The Hudson (1994) IRTF sample, reported in his Table 3, a list of 21 objects with a distance smaller than 8000 km s^{-1}, again originating from Burstein (1990). The calibration is made using the nine Aaronson et al. (1986) clusters which are located inside the region considered. The random error in this calibration is 2%.

(3) The Giovanelli (1995) sample, an updated version of the Giovanelli et al. (1995) catalogue containing 23 cluster peculiar velocities obtained by the IRTF method. The calibration comes from those clusters which lie at a distance larger than 4000 km s^{-1}.

The results of the CVFD test for these samples have been already shown in Figure 6. In Table 5 we report the values of the rms velocity estimated from the line–of–sight observational peculiar velocities with the same method previously applied to the composite sample. We note that, while the results from the IRTF and D_n–σ Hudson (1994) catalogues are fairly consistent both with

[table]

Table 4. Results for the composite sample. The different simulation rms line–of–sight velocity values, σ_v (in $\mathrm{km\,s^{-1}}$), before (Column 2) and after (Column 3) convolution with the observational uncertainties of the composite sample. Also reported is the fraction $\mathcal{F}_{\sigma_v}$ of the extracted samples (Column 4) having σ_v falling within the 1σ observational range. Columns 5, 6 and 7 refer to the fractions of extracted samples for which the measured cumulative velocity frequency distribution $P(>v)$ assumes a value within 1σ from the observed data, computed for $v = 0.5\sigma_v$ ($\mathcal{F}_{0.5}$), $v = 1\sigma_v$ ($\mathcal{F}_1$) and $v = 2\sigma_v$ ($\mathcal{F}_2$), respectively.

Model	σ_v (unconv.)	σ_v (conv.)	$\mathcal{F}_{\sigma_v}$	$\mathcal{F}_{0.5}$	$\mathcal{F}_1$	$\mathcal{F}_2$
Composite (D_n–σ & IRTF)		725 ± 60				
SCDM	664	797 ± 78	0.413	0.187	0.133	0.543
CHDM	467	633 ± 66	0.293	0.548	0.505	0.276
OCDM02	93	423 ± 61	$< 10^{-3}$	$< 10^{-3}$	0.002	0.021
OCDM03	98	434 ± 62	0.001	$< 10^{-3}$	0.002	0.035
OCDM04	197	465 ± 60	0.002	0.013	0.009	0.039
OCDM06	415	592 ± 63	0.123	0.503	0.379	0.183
OCDM08	574	718 ± 72	0.594	0.373	0.390	0.507
ΛCDM02	247	492 ± 59	0.004	0.066	0.029	0.069
ΛCDM03	388	589 ± 63	0.115	0.488	0.369	0.173
ΛCDM04	504	666 ± 68	0.450	0.499	0.523	0.371
ΛCDM06	570	720 ± 72	0.597	0.358	0.382	0.506
ΛCDM08	623	762 ± 73	0.546	0.235	0.205	0.558

each other and with the value obtained from the consolidated catalogue ($646 \pm 102\,\mathrm{km\,s^{-1}}$ and $688 \pm 82\,\mathrm{km\,s^{-1}}$ versus $725 \pm 60\,\mathrm{km\,s^{-1}}$), the value of σ_v from the Giovanelli (1995) sample is much smaller, $356 \pm 37\,\mathrm{km\,s^{-1}}$. The resulting discrepancy has a high confidence level, ($\sim 3\sigma$) for both the D_n–σ and the IRTF Hudson subsamples.

In order to compare these results with the cosmological models, we convolve the simulated cluster velocities with the observational uncertainties for each sample separately: the resulting σ_v are shown in Table 5. These values and their errors are the mean and the 1σ scatter over an ensemble of 20,000 samples, respectively. Also reported is the fraction $\mathcal{F}_{\sigma_v}$ of those samples which measure a value of the rms velocity σ_v within the 1σ observational band. Once again, the results for the D_n–σ and the IRTF Hudson (1994) samples are very similar and in good agreement with the results for the composite catalogue: the only models we can reject on the basis of this analysis are OCDM with $\Omega_0 \leq 0.4$ and ΛCDM02.

The situation is radically different when the Giovanelli (1995) data are used. Due to the smaller errors reported for this sample, the discriminatory power of the test is very high and only two models survive: namely OCDM04 and ΛCDM02. Note that these models are both rejected by either the composite or the Hudson (1994) samples.

4.3.3 Results for the BPS reconstructed velocities

The results of the comparison between models and BPS cluster velocities are also shown in Table 5, where we report the BPS rms line-of-sight velocity $\sigma_v = 522 \pm 15$ km s^{-1}, estimated with the same convolution method that was previously applied to the observational samples. Following the same procedure as before, we find that the only models having a non–negligible fraction of "good" observers are CHDM, ΛCDM04 and OCDM06. It is interesting to note that now the SCDM model is rejected at a high significance level, in agreement with the result based on the Giovanelli (1995) data. Note that none of the models that satisfy the BPS velocities are the same time accepted by the analysis based on the Giovanelli data, but are accepted on the basis of the Hudson and composite samples.

It is worth recalling here that the high discriminatory power of such reconstructed data is due to both their large number and their small errors. However, as we already mentioned, such errors include observational as well as intrinsic uncertainties related to the reconstruction procedure but they do not account for possible systematic effects related to the validity of the linear biasing assumption on which the reconstruction method relies. It is wise, therefore, to interpret these results only as indications, but indications which are, nevertheless, in agreement with the analysis of the composite and Hudson data.

[table]

Table 5. Results for single samples. The values of the simulation rms velocities σ_v (in $\mathrm{km\,s^{-1}}$), evaluated for one–dimensional data after convolution with the observational uncertainties, and the fraction $\mathcal{F}_{\sigma_v}$ of the extracted samples having σ_v falling within the 1σ observational range are reported for the Hudson (1994) D_n–σ catalogue (Columns 2 and 3), for the Hudson (1994) IRTF catalogue (Columns 4 and 5), for the Giovanelli (1995) IRTF catalogue (Columns 6 and 7) and for the Branchini et al. (1995) reconstructed velocities (Columns 8 and 9).

Sample	Hudson D_n–σ		Hudson IRTF		Giovanelli IRTF		Branchini et al.	
Objects	16*		21		23		280	
Model	σ_v	$\mathcal{F}_{\sigma_v}$	σ_v	$\mathcal{F}_{\sigma_v}$	σ_v	$\mathcal{F}_{\sigma_v}$	σ_v	$\mathcal{F}_{\sigma_v}$
Observed	646 ± 102		688 ± 82		356 ± 37		522 ± 15	
SCDM	786 ± 72	0.303	781 ± 73	0.343	702 ± 64	$< 10^{-3}$	703 ± 64	0.003
CHDM	625 ± 61	0.885	614 ± 60	0.400	513 ± 50	0.001	512 ± 50	0.220
OCDM02	407 ± 45	0.003	395 ± 47	$< 10^{-3}$	215 ± 27	0.003	214 ± 27	$< 10^{-3}$
OCDM03	418 ± 47	0.008	405 ± 50	$< 10^{-3}$	222 ± 27	0.004	222 ± 28	$< 10^{-3}$
OCDM04	454 ± 49	0.042	440 ± 49	$< 10^{-3}$	284 ± 29	0.264	284 ± 30	$< 10^{-3}$
OCDM06	581 ± 56	0.735	572 ± 56	0.169	465 ± 43	0.008	464 ± 43	0.107
OCDM08	707 ± 68	0.727	700 ± 67	0.659	616 ± 57	$< 10^{-3}$	616 ± 57	0.055
ΛCDM02	482 ± 50	0.111	469 ± 50	0.003	331 ± 33	0.672	330 ± 32	$< 10^{-3}$
ΛCDM03	578 ± 55	0.724	570 ± 57	0.163	458 ± 43	0.013	460 ± 44	0.093
ΛCDM04	654 ± 62	0.896	646 ± 62	0.575	551 ± 50	$< 10^{-3}$	551 ± 50	0.199
ΛCDM06	709 ± 67	0.718	703 ± 68	0.650	613 ± 57	$< 10^{-3}$	612 ± 57	0.059
ΛCDM08	751 ± 68	0.483	746 ± 69	0.513	668 ± 60	$< 10^{-3}$	667 ± 60	0.010

* the data of Cen45 is discarded.

5 DISCUSSION

This work was devoted to a thorough investigation of the velocity field as traced by galaxy clusters. We have focussed our attention on understanding whether such large–scale flows can be usefully employed to constrain the values of the cosmological parameters Ω_0 and Ω_Λ.

We have used a simulation technique based on the Zel'dovich approximation, first testing this method carefully by comparing its results with a full N–body code. We have introduced two different definitions of velocity in our simulations. The first, linear, definition (LIN) amounts to the assumption that the particle velocities are given by the gradient of the linear gravitational potential estimated at the initial (Lagrangian) particle position. In the second, quasi–linear, definition (ZEL) the particle velocity is estimated through the gradient of the (Zel'dovich–evolved) potential evaluated at the final (Eulerian) particle position. We compared the cluster velocity fields corresponding to these two prescriptions with that obtained from the N–body simulation by applying different statistical tests, such the velocity frequency distribution, the velocity correlation function and the bulk flow. From this analysis we conclude that the quasi–linear definition (ZEL) for the cluster velocities is consistent with N–body results for scales $\gtrsim 10 - 20\,h^{-1}$Mpc. This is true even for high–normalization spectra, $\sigma_8 \simeq 1$, when a substantial degree of non–linearity is present on the cluster mass scale.

In the framework of the CDM cosmogony, we considered models with $0.2 \leq \Omega_0 \leq 1$, both with flat (ΛCDM) and open (OCDM) geometry. We also considered the $\Omega_0 = 1$ Cold+Hot DM (CHDM) model with 30% of hot component. For each model, we ran a single realization within a large enough box, $960\,h^{-1}$Mpc on a side, to render any effect of cosmic variance entirely negligible.

We first compared predictions of the relevant models for both the 3D cluster velocity frequency distribution (VFD), $P(v)$, and the velocity correlation function, $\xi_v(r)$. These statistics have been shown to possess an intrinsic discriminatory power between such models. This is particularly true for the OCDM models which have rather different VFDs and velocity correlations. The differences are instead smaller in the case of the ΛCDM models, with the only exception of the $\Omega_0 = 0.2$ case. We also found, in agreement with previous analyses (e.g. Bahcall et al. 1994a), that all the models display a $P(v)$ which is well fitted by a Maxwellian distribution.

In order to constrain the models we compared their predictions with available cluster velocity data. As a

first test we computed the probability of having observers with the Local Group characteristics (i.e. similar local velocity and density contrast). The comparison for the bulk flow statistic has been made with the results recently obtained by Branchini et al. (1995), based on an iterative procedure used to reconstruct the cluster real space positions and peculiar velocities. Both analyses show that the only models which can be ruled out at a rather high confidence level are the OCDM ones with $\Omega_0 < 0.4$. Note that the bulk flow measured by Branchini et al. (1995) at $150\,h^{-1}$Mpc has a much lower amplitude (and much better alignment with the CMB dipole) than that obtained by Lauer & Postman (1994), which however used cluster peculiar velocities measured directly using a distance indicator based on the properties of brightest cluster galaxies. We found, in agreement with other analyses, that the Lauer & Postman (1994) bulk flow is an extremely rare event in most of our models, although in the case of ΛCDM models (particularly for those with $\Omega_\Lambda = 0.3$ and 0.4) there is a small but non–negligible probability of obtaining the sample amplitude as the Lauer & Postman bulk flow.

As a further test, we computed the 1D cumulative velocity frequency distribution (CVFD) and the velocity dispersion σ_v. We constructed a composite catalogue by collecting observed cluster velocities from different data sets, based on both D_n–σ and IRTF methods (see Table 2). The final observational sample used in the analysis contains 62 objects. We took into account the large observational uncertainties by convolving the simulated cluster velocities with the error reported in the source catalogues. This convolution broadens the velocity distributions and increases the values of σ_v, thus reducing the differences between the models. In this way the possibility of constraining the Ω_0 and Ω_Λ parameters is largely reduced. The low–Ω_0 models are again disfavoured, particularly in the case of open models, for which $\Omega_0 > 0.4$ is required to fit the data; the ΛCDM02 model is also in trouble, while ΛCDM08 and SCDM have systematically fewer clusters with high velocity than in the observational sample.

In order to check whether our composite sample is affected by biases associated with its heterogenous composition, we considered also three smaller samples directly taken from the literature: the D_n–σ and the IRTF Hudson (1994) catalogues and the IRTF Giovanelli (1995) catalogue. The paucity of the data and the large uncertainties affecting the two Hudson samples yield less stringent results, but in agreement with the analysis of the composite catalogue (cf. Tables 4 and 5). Note that the two Hudson samples contain data obtained from different distance indicators (D_n–σ and IRTF relations). The similarity of the results therefore seems to indicate that there is not an intrinsic bias introduced by the technique adopted in obtaining the data. On the other hand, the results from the Giovanelli (1995) sample are completely different: this catalogue is dominated by clusters with very small velocities and the resulting velocity dispersion is consequently also very small. In this case, the only models in agreement with the data are OCDM04 and ΛCDM02, which were excluded by the analysis of the composite and of the Hudson samples.

The discrepancy between the Giovanelli data and all other studies was already noted by the authors themselves (see, e.g., Giovanelli et al. 1995). They claim that their results are more reliable for the following reasons:

(1) they used a homogenous galaxy sample, which provides a full coverage of the sky;
(2) they adopted a different Tully–Fisher template relation, obtained from an extensive study of clusters;
(3) they applied an internal extinction correction which depends on the luminosity and allows for larger flux corrections.

On the other hand, a possible bias for the Giovanelli sample might have arisen from their estimate of the IRTF relation zero–point. They adopted that of the mean relation obtained from all clusters with $cz > 4000$ km s^{-1} in the CMB frame, since, as they argue, at such distances small peculiar velocities translate into small magnitude offsets, and that possible bulk flows do not affect the mean IRTF relation since the clusters are isotropically distributed. However, since the number of available clusters is small (~ 15), even if they are random samplers of an isotropic distribution, they could introduce shot–noise deviations from the 'isotropic' zero–point value. A second concern is related to the use of the CMB rest–frame. If there is a bulk flow, in which the LG participates, then, by using this frame the sampled volume becomes elongated along the direction of the bulk flow, compared to a spherically symmetric distribution.

We have also analysed the CVFD for the BPS reconstructed cluster velocities, which represents a completely independent data set. It turns out that such velocities pose the most stringent constraints on the different cosmological models (cf. Table 5). Since, however, the BPS velocities are not truly observational but depend on various assumptions we choose not to present

the above results as final and firm conclusions. In particular, the assumption of a linear biasing relationship which is independent of spatial position, may well not be valid. Our ignorance about the possible cluster–by–cluster variation of the biasing parameter would increase the individual reconstructed velocity uncertainties. For these reasons, we prefer at present to consider these results only as circumstantial evidence in support of inferences made on the basis of the composite and Hudson data.

6 CONCLUSIONS

The first definite conclusion of this work is that our method to simulate the cluster velocity field, which is based on an optimized version of the Zel'dovich approximation, is easy to implement, cheap from the computational point of view and fully reliable, as shown by the comparison with the results of a full N–body code.

As for the comparison between observational data and numerical simulations on cluster peculiar velocities is concerned, our main findings can be sketched as follows.

(a) The bulk flow analysis performed on the Branchini et al. (1995) data and the probability of reproducing the Local Group characteristics rule out only open CDM models with $\Omega_0 < 0.4$. We also confirm that the Lauer & Postman (1994) high bulk velocity, at an effective depth of $\sim 100\,h^{-1}$Mpc, is an extremely unlikely event in all the $\Omega_\Lambda = 0$ models. However, in $\Omega_\Lambda \neq 0$ models there is a small but non–negligible probability of reproducing this observation.

(b) The VFD analysis based on a composite sample of 62 cluster velocities, obtained both with IRTF and D_n–σ methods, rules out open CDM models with $\Omega_0 \leq 0.4$ and the ΛCDM model with $\Omega_0 = 0.2$. Standard CDM and ΛCDM with $\Omega_0 = 0.8$ are disfavoured, although only marginally. Similar results are found by applying the same test on the two Hudson (1994) catalogues, based on the IRTF and D_n–σ relations, respectively: no systematic bias appears to be introduced by the different distance indicators.

(c) The application of the VFD test to the IRTF Giovanelli (1995) sample gives completely different results. The smaller velocities and errors reported in this sample are such that the only surviving models are the open CDM with $\Omega_0 = 0.4$ and the ΛCDM with $\Omega_0 = 0.2$.

(d) We found also that the above two models, which are consistent with the Giovanelli data, are strongly disfavoured by an analysis of the Branchini et al. (1995) reconstructed velocities, in agreement with the interpretation of the Hudson and composite sample analyses.

As a concluding remark, we would like to stress the importance of identifying the reasons for the puzzling discrepancy between different data sets. Our analysis has shown that a small, but accurate, sample of cluster peculiar velocities, like that of Giovanelli (1995), can put rather stringent constraints on different DM models. We therefore consider the analysis presented here as proving the potential of cluster velocity considerations, and look forward to the availability of newer and more precise cluster velocity measurements.

ACKNOWLEDGMENTS

LM and PTB thank Italian MURST for partial financial support. PTB also acknowledges CUC for partial financial support. MP has been supported by an EEC *Human Capital and Mobility* fellowship. PC is a PPARC Advanced Research Fellow. EB and PTB acknowledge the EC for financial support during their visit in QMWC and thank QMWC for its hospitality. This work has been partly supported by funds originating from the *EC* Human Capital and Mobility Network (Contract Number CHRX–CT93–0129). We thank Riccardo Giovanelli for providing us with his cluster redshifts prior to publication and for useful comments.

REFERENCES

Aaronson M., Bothun G., Mould J., Huchra J., Schommer R.A., Cornell M.E., 1986, ApJ, 302, 536

Aaronson M., et al., 1989, ApJ, 338, 654

Bahcall N.A., Cen R., Gramann M., 1994a, ApJ, 430, L13

Bahcall N.A., Gramann M., Cen R., 1994b, ApJ, 436, 23

Bennett C.L., et al., 1994, ApJ, 436, 423

Borgani S., Plionis M., Coles P., Moscardini L., 1995, MNRAS, in press, preprint astro–ph/9505050 (Paper I)

Branchini E., Plionis M., 1995, ApJ, in press

Branchini E., Plionis M., Sciama D.W., 1995, ApJL, submitted [BPS]

Bucher M., Goldhaber A.S., Turok N., 1995, Phys. Rev. D., 53, 3314

Burstein D., 1990, Mark II compilation of peculiar velocities, privately circulated

Cen R., Bahcall N.A., Gramann M., 1994, ApJ, 437, L51

Chaboyer B., Kernan P.J., Krauss L.M., Demarque P., 1995, preprint astro-ph/9509115

Coles P., Ellis G.F.R., 1994, Nature, 370, 609

Coles P., Melott A.L., Shandarin S.F., 1993, MNRAS, 260, 765

Croft R.A.C., Efstathiou G., 1994, MNRAS, 268, L23

Croft R.A.C., Efstathiou G., 1995, in eds. Muecket J., et al., Proc. of the Potsdam Meeting on Large–scale structure in the universe, in press

da Costa et al., 1995, in eds. Balkowski C., Maurogordato S., Tao C. & Trân Thanh Vân J., Proc. of the Moriond Astrophysics Meeting on Clustering in the Universe, in press

Dekel A., 1994, ARA&A, 32, 99

Efstathiou G., Bond J.R., White S.D.M., 1992, MNRAS, 258, 1p

Efstathiou G., Sutherland W.J., Maddox S.J., 1990, Nat, 348, 705

Ellis G.F.R., Lyth D.H., Mijic M.B., 1991, Phys. Lett., B271, 52

Faber S.M., Wegner G., Burstein D., Davies R., Dressler A., Lynden–Bell D., Terlevich R., 1989, ApJSS, 69, 763

Feldman H.A., Watkins R., 1994, ApJ, 430, L17

Giovanelli R., 1995, in eds. Bonometto S., Primack J., & Provenzale A., Proc. of the International School of Physics Enrico Fermi, Course CXXXII: Dark Matter in the Universe, in press

Giovanelli R., Haynes M.P., Chamaraux P., da Costa L.N., Freudling W., Salzer J.J., Wegner G., 1995, in ed. Kafatos M., Proc. of the IAU Symp. Examining the Big Bang and Diffuse Background Radiation, in press

Górski K., 1988, ApJ, 332, L7

Górski K.M., Ratra B., Sugiyama N., Banday A.J., 1995, ApJ, 444, L65

Górski K., et al., 1989, ApJ, 344, 1

Górski K., et al., 1994, ApJ, 430, L89

Gramann M., Bahcall N.A., Cen R., Gott J.R., 1995, ApJ, 441, 449

Haenhelt M.G., Tegmark M., 1995, preprint astro–ph/9507077

Han M., Mould J.R., 1992, ApJ, 396, 453

Hockney R.W., Eastwood J.W., 1981, Computer Simulations Using Particles. McGraw–Hill, New York

Holtzman J.A., 1989, ApJS, 71, 1

Hudson M.J., 1994, MNRAS, 266, 475

Hudson M.J., Dekel A., Courteau S., Faber S.M., Willick J.A., 1995, MNRAS, 274, 305

Jaffe A., Kaiser N., 1994, preprint astro–ph/9408046

Kaiser N., 1988, MNRAS, 239, 149

Kofman L., Bertschinger E., Gelb J.M., Nusser A., Dekel A., 1994, ApJ, 420, 44

Kofman L., Gnedin N.Y., Bahcall N.A., 1993, ApJ, 413, 1

Kogut A., et al., 1993, ApJ, 419, 1

Kolokotronis V., Plionis M., Coles P., Borgani S., Moscardini L., 1995, MNRAS, submitted

Lauer T., Postman M., 1994, ApJ, 425, 418

Liddle A.R., Lyth D.H., Roberts D., Viana P.T.P., 1995, preprint astro–ph/9506091

Linde A., Mezhlumian A., 1995, preprint astro–ph/9506017

Lucchin F., Matarrese S., 1985, Phys. Lett., 164B, 282

Lucey J., Carter D., 1988, MNRAS, 235, 1177

Mathewson D.S., Ford V.L., Buchhorn M., 1992, ApJSS, 81, 413

Melott A.L., Pellman T.F., Shandarin S.F., 1994, MNRAS, 269, 626

Moscardini L., Tormen G., Matarrese S., Lucchin F., 1995, ApJ, 442, 469

Mould J.R., Akeson R.L., Bothun G.D., Han M., Huchra J.P., Roth J., Schommer R.A., 1993, ApJ, 409, 14

Mould J.R., et al., 1991, ApJ, 383, 467

Peacock J.A., Dodds S.J., 1994, MNRAS, 267, 1020

Peebles P.J.E., 1993, Principles of Physical Cosmology. Princeton University Press, Princeton

Plionis M., Borgani S., Moscardini L., Coles P., 1995, ApJ, 441, L57

Primack J.R., 1995, Plenary Talk at Snowmass 1994, preprint astro–ph/9503020

Ratra B., Peebles P.J.E., 1994, ApJ, 432, L5

Ratra B., Peebles P.J.E., 1995, Phys. Rev., D52, 1837

Reeves H., 1994, Rev. Mod. Phys., 66, 193

Regős E., Szalay A.S., 1989, ApJ, 345, 627

Riess A., Press W., Kirshner R., 1995, ApJ, 438, L17

Sasaki M., Tanaka T., Yamamoto K., Yokoyama J., 1993, Phys. Lett., B317, 510

Shandarin S.F., Zel'dovich Ya.B., 1989, Rev. Mod. Phys., 61, 185

Shi X., 1995, ApJ, 446, 637

Stompor R., Górski K.M., Banday A.J., 1995, MNRAS, in press, preprint astro–ph/9502035 (SGB)

Strauss M.A., Cen R., Ostriker J.P., Lauer T.R., Postman M., 1995, ApJ, 446, 507

Strauss M.A., Davis, M., 1988, in Rubin V.C., Coyne G., eds, Large Scale Motions in the Universe: A Vatican Study Week. Princeton Univ. Press, Princeton, p. 255

Strauss M.A., Willick J.A., 1995, Phys Rep., 261, 271

Sugiyama N., 1995, preprint astro–ph/9503089

Sunyaev R., Zel'dovich Ya.B., 1980, MNRAS, 190, 413

Tegmark M., Bunn E.F., Hu W., 1994, ApJ, 434, 1

Tini Brunozzi P., Borgani S., Plionis M., Moscardini L., Coles P., 1995, MNRAS, in press, preprint astro–ph/9506110

Tormen G., Moscardini L., Lucchin F., Matarrese S., 1993, ApJ, 411, 16

Yahil A., Strauss M.A., Davis M., Huchra J.P., 1991, ApJ, 372, 380

Yamamoto K., Bunn E.F., 1995, preprint astro–ph/9508090

Zel'dovich Ya.B., 1970, A&A, 5, 84

FIGURE CAPTIONS

Figure 1. Comparison of the projected velocity fields traced by clusters in a N–body simulation (PM, upper row) and in Zel'dovich simulations with two different definitions for the velocity: ZEL (central row) and LIN (bottom row). The simulations have a box–size of $320\,h^{-1}$Mpc and the same CHDM initial conditions. The slice is $60\,h^{-1}$Mpc thick. A smoothing by a Gaussian filter with width $20\,h^{-1}$Mpc is applied. Two different stages are shown: $\sigma_8 = 0.67$ (left column) and $\sigma_8 = 1$ (right column).

Figure 2. Comparison of the results of the application of different statistical tests to the cluster velocity fields obtained in a N–body simulation (PM, solid lines) and in Zel'dovich simulations with two different definitions for the velocity: ZEL (dotted lines) and LIN (dashed lines). Upper row: the 3D velocity frequency distribution $P(v)$. Central row: the velocity correlation function ξ_v (in km s^{-1}) as a function of the distance r (in h^{-1}Mpc). Bottom row: the bulk flow velocity $V_{\rm bulk}$ (in km s^{-1}) as a function of the distance r (in h^{-1}Mpc). Two different stages are shown: $\sigma_8 = 0.67$ (left column) and $\sigma_8 = 1$ (right column).

Figure 3. The frequency distribution $P(v)$ for the 3D cluster velocity field for different models: SCDM and CHDM models (top left), OCDM models (top right), ΛCDM models (bottom left). The dashed lines in the top left panel show the Maxwellian curves fitting the distributions.

Figure 4. The velocity correlation function ξ_v (in km s^{-1}) as a function of the distance r (in h^{-1}Mpc) for different models: SCDM and CHDM models (top left), OCDM models (top right), ΛCDM models (bottom left).

Figure 5. The bulk flow velocity $V_{\rm bulk}$ (in km s^{-1}) as a function of the distance r (in h^{-1}Mpc) for different models: SCDM and CHDM models (top left), OCDM models (top right), ΛCDM models (bottom left). The dashed region represents the 1σ strip allowed by the Branchini et al. (1995) data.

Figure 6. The 1D cumulative velocity frequency distribution $P(>v)$ of our composite catalogue (solid line) is compared to that of the Hudson (1994) IRTF sample (short–dashed line), of the Hudson (1994) D_n–σ sample (long–dashed line), of the Giovanelli (1995) sample (dotted line) and of the Branchini et al. (1995) reconstructed data (dotted–dashed line). Error bars, plotted only for the composite and Giovanelli samples, correspond to the 2σ scatter over 20,000 resamplings.

Figure 7. The 1D cumulative velocity frequency distribution $P(>v)$ for different models compared with that resulting from our composite observational catalogue (filled circles with 2σ uncertainties obtained as scatter over an ensemble consisting of 20,000 resamplings of the original data). The model curves are the mean of 20,000 samples of 62 randomly selected clusters whose velocities are convolved with the observational errors. The panels refer to SCDM and CHDM models (top left), OCDM models (top right) and ΛCDM models (bottom left).

PM σ_8=0.67

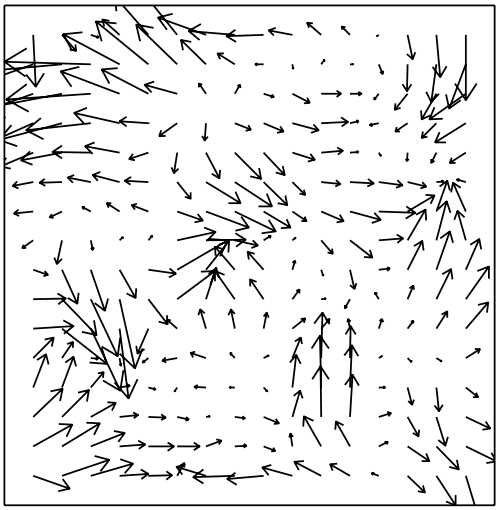

PM σ_8=1.

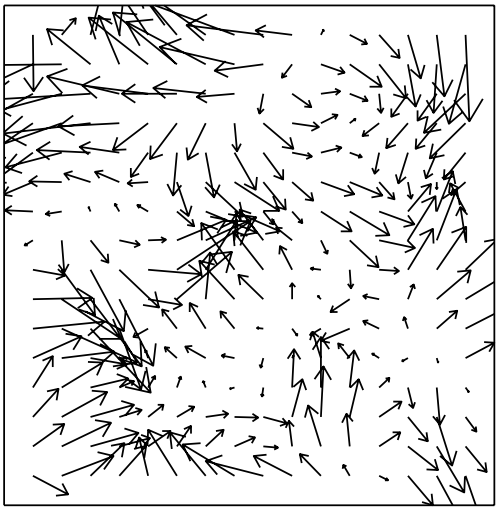

ZEL σ_8=0.67

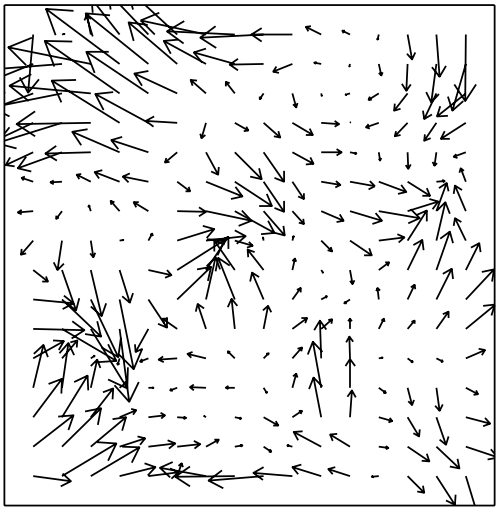

ZEL σ_8=1.

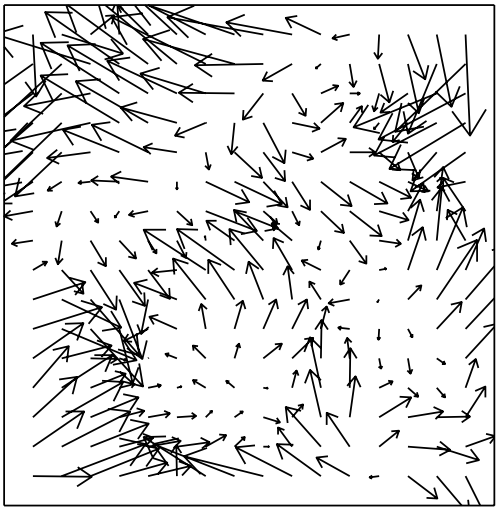

LIN σ_8=0.67

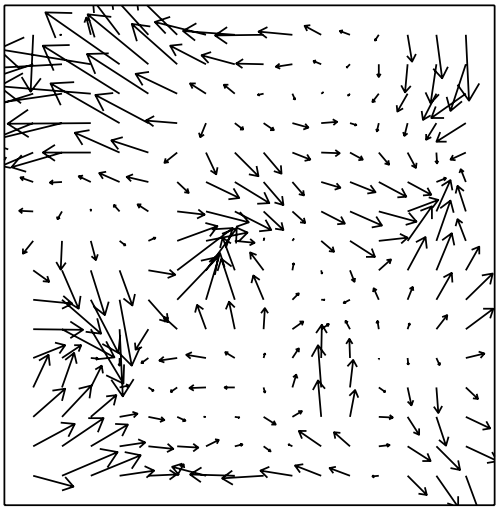

LIN σ_8=1.

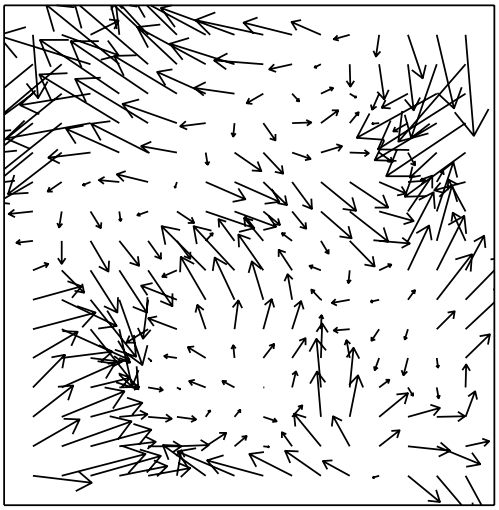

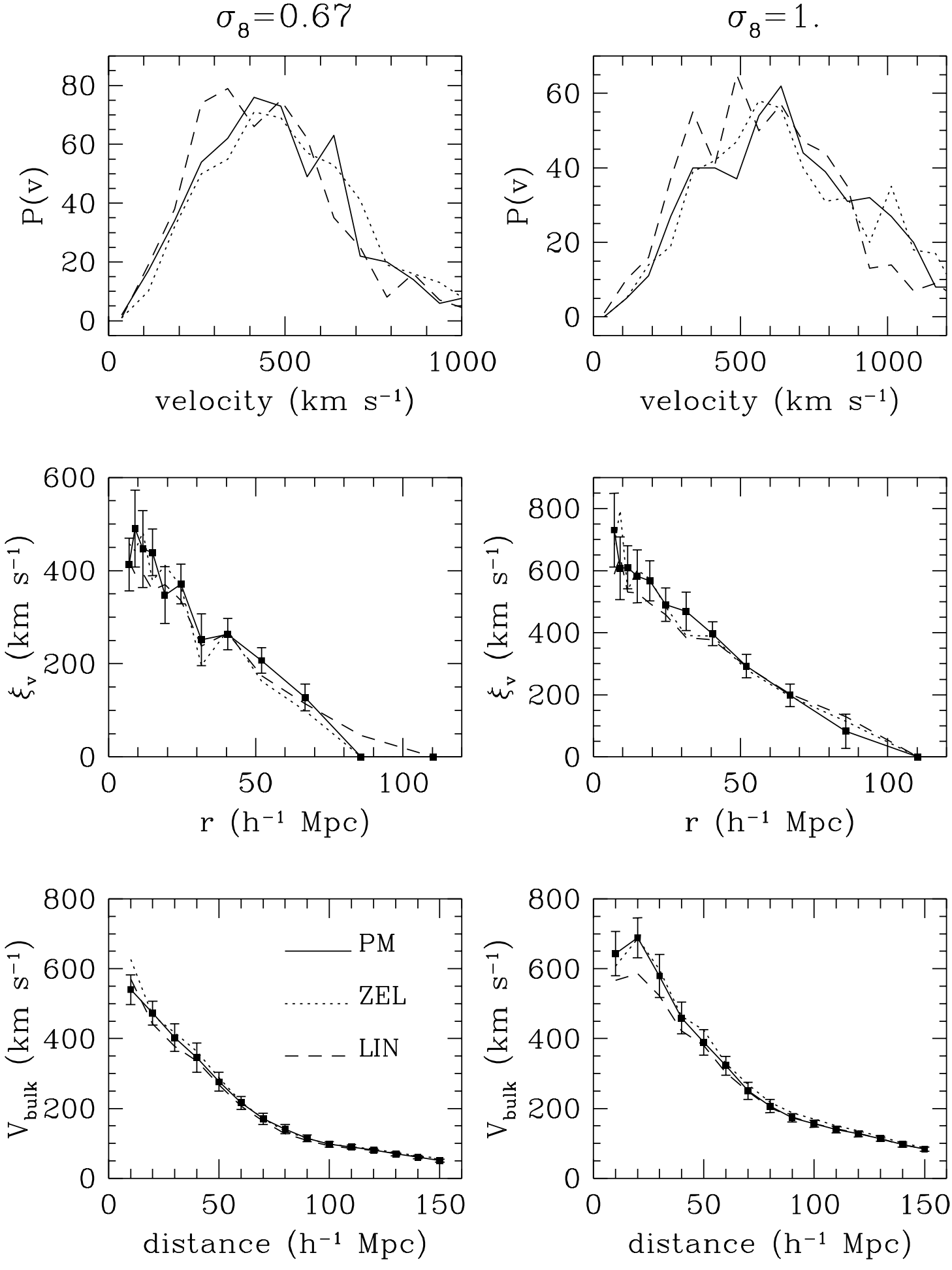
σ_8=0.67
σ_8=1.
P(v)
velocity (km s^{-1})
ξ_v (km s^{-1})
r (h^{-1} Mpc)
V_{bulk} (km s^{-1})
distance (h^{-1} Mpc)
PM
ZEL
LIN

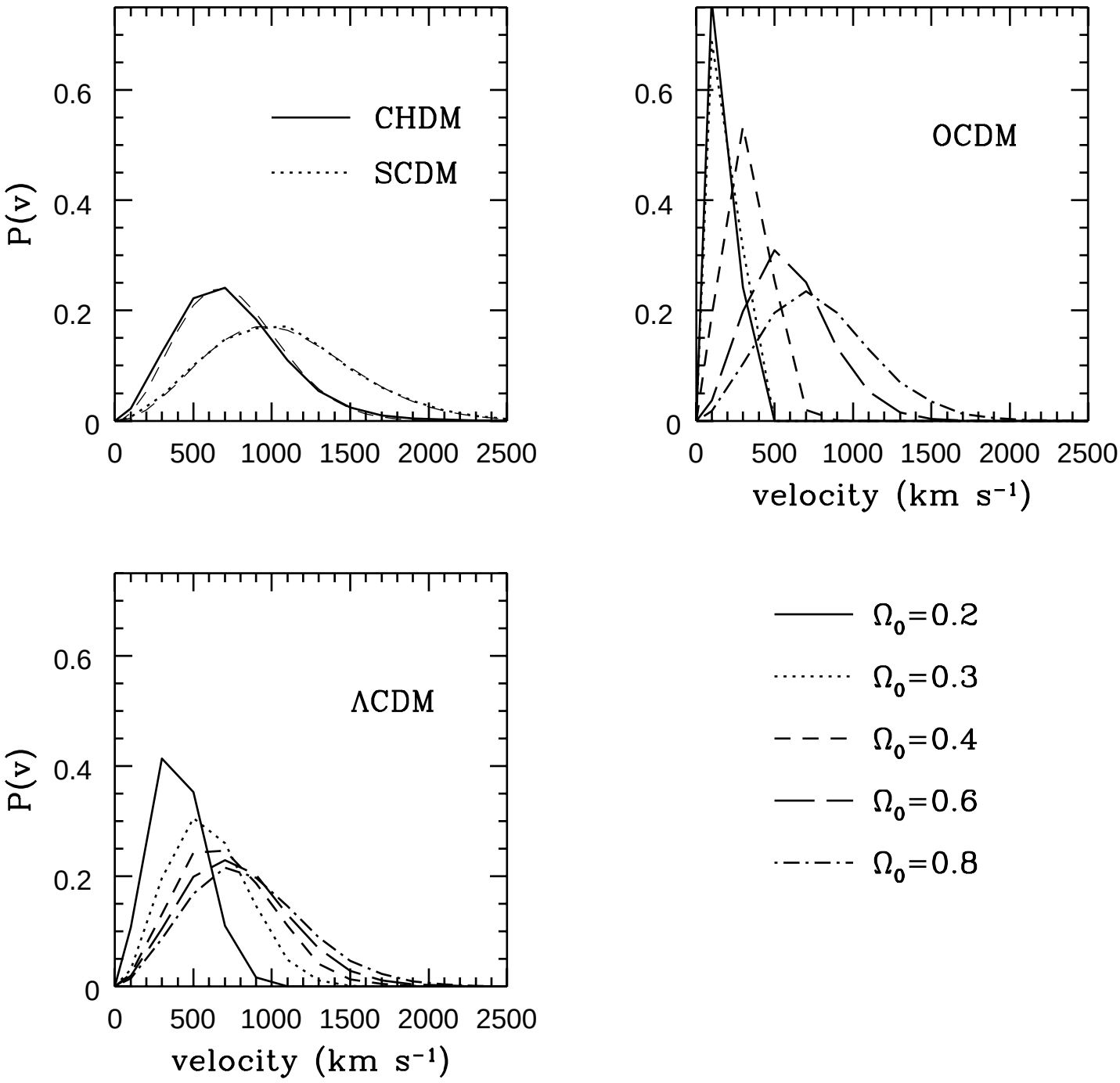
CHDM
SCDM
OCDM
ΛCDM
P(v)
velocity (km s⁻¹)
0
0.2
0.4
0.6
0
500
1000
1500
2000
2500
Ω₀=0.2
Ω₀=0.3
Ω₀=0.4
Ω₀=0.6
Ω₀=0.8

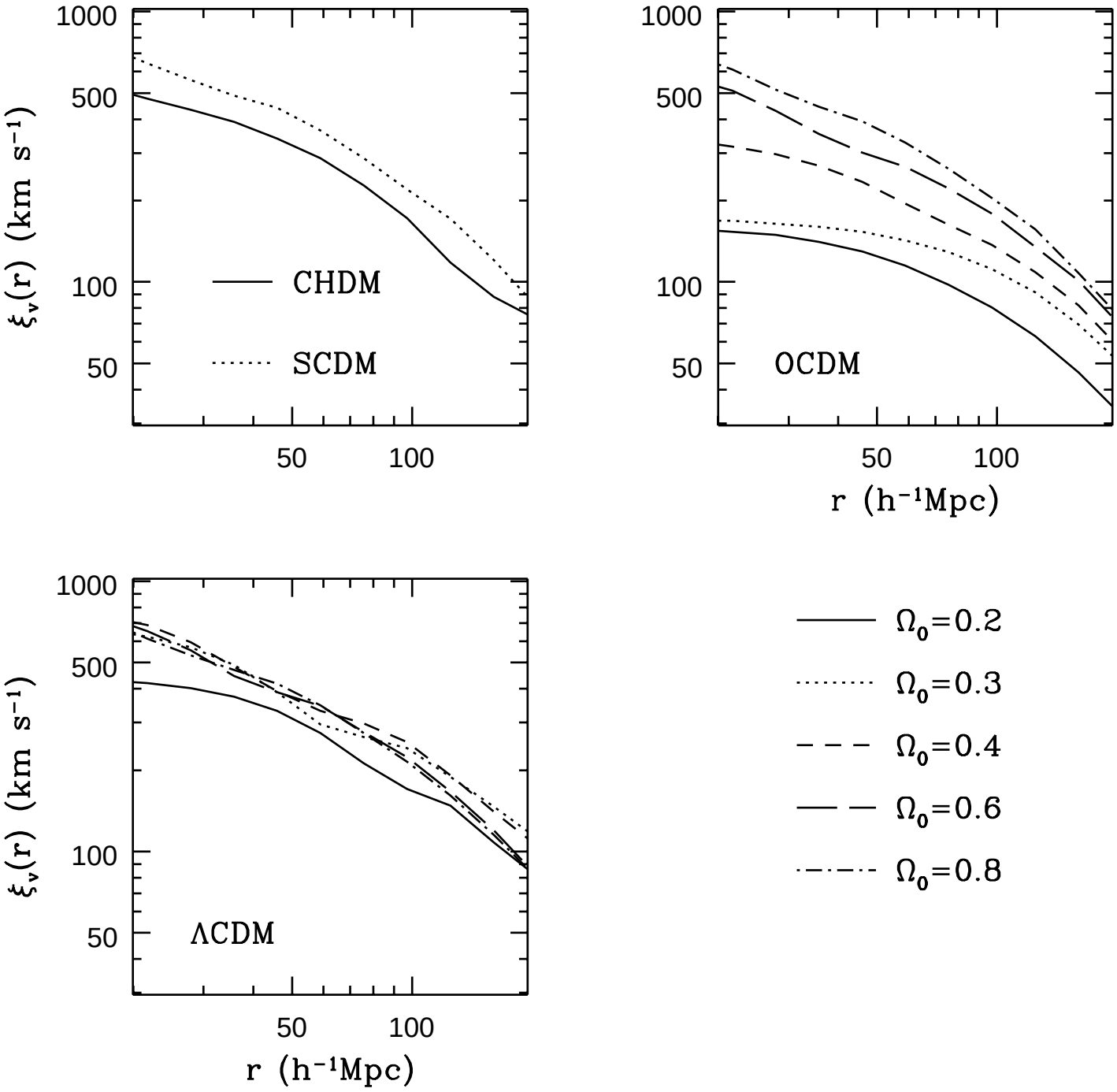
1000
500
100
50
$\xi_v(r)$ (km s^{-1})
CHDM
SCDM
50
100
OCDM
r (h^{-1}Mpc)
ΛCDM
Ω_0=0.2
Ω_0=0.3
Ω_0=0.4
Ω_0=0.6
Ω_0=0.8

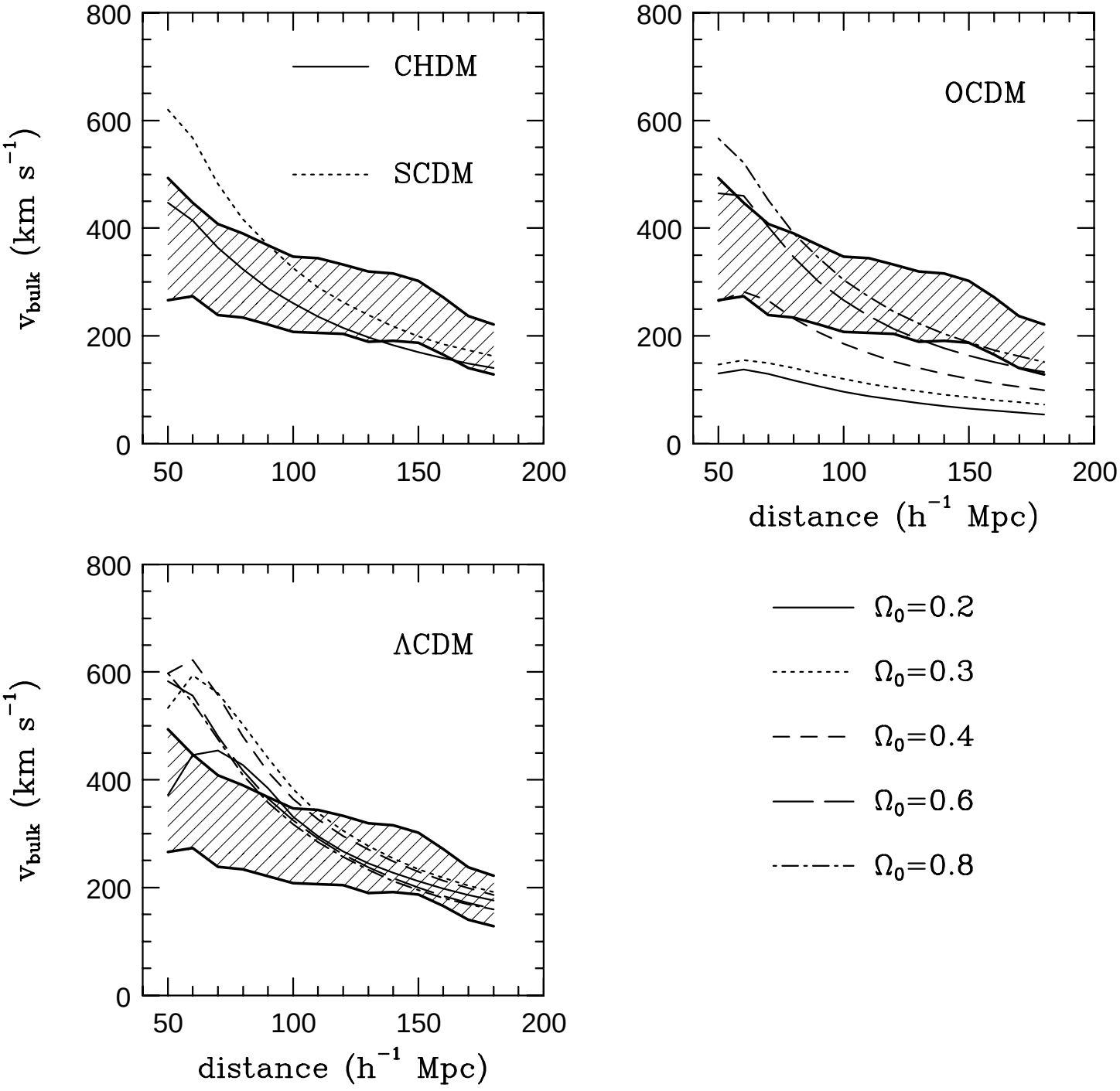
CHDM
SCDM
OCDM
ΛCDM
v_{bulk} (km s^{-1})
distance (h^{-1} Mpc)
0
200
400
600
800
50
100
150
200
Ω_0=0.2
Ω_0=0.3
Ω_0=0.4
Ω_0=0.6
Ω_0=0.8

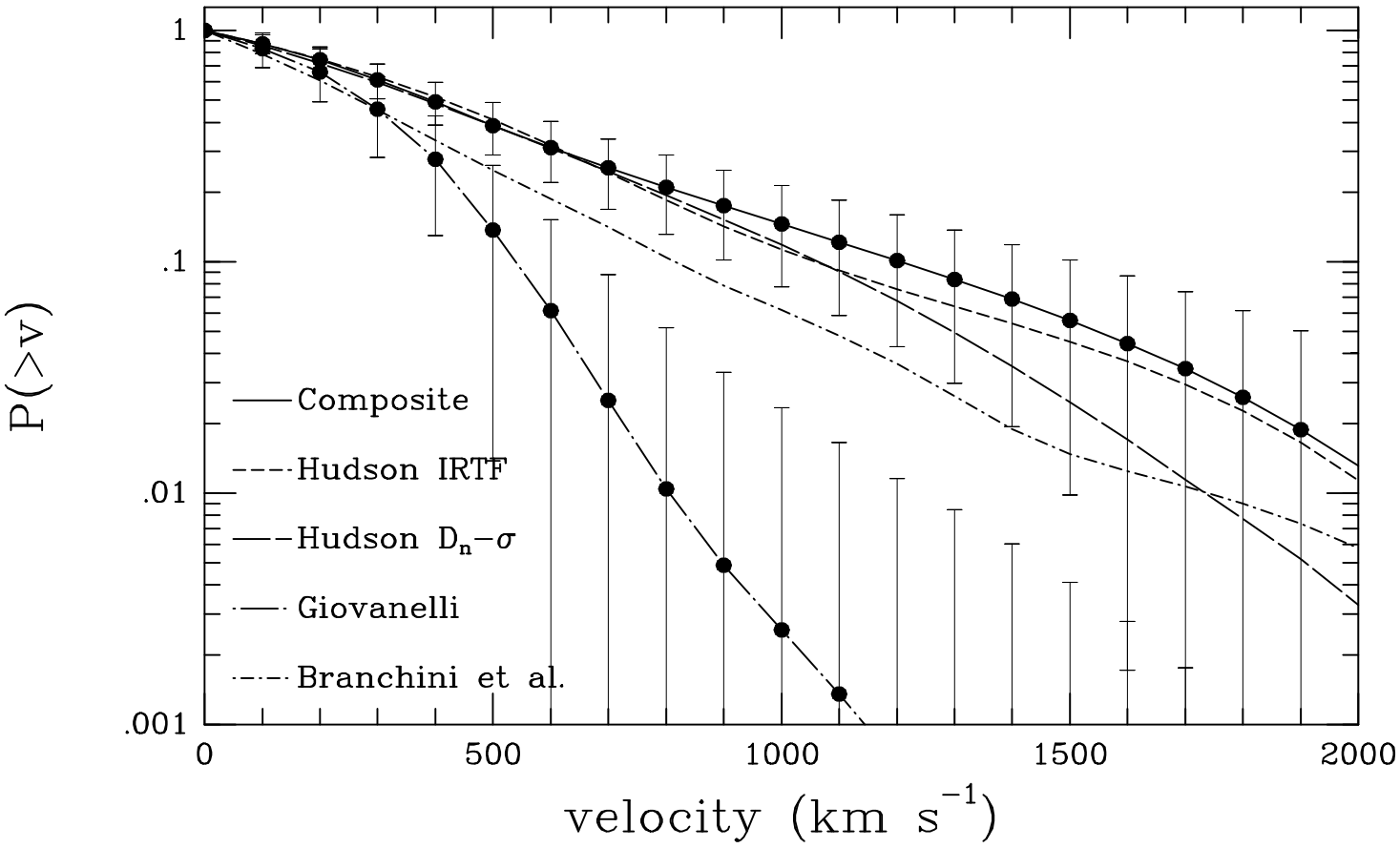
1
.1
.01
.001
P(>v)
0
500
1000
1500
2000
velocity (km s^{-1})
Composite
Hudson IRTF
Hudson $D_n-\sigma$
Giovanelli
Branchini et al.

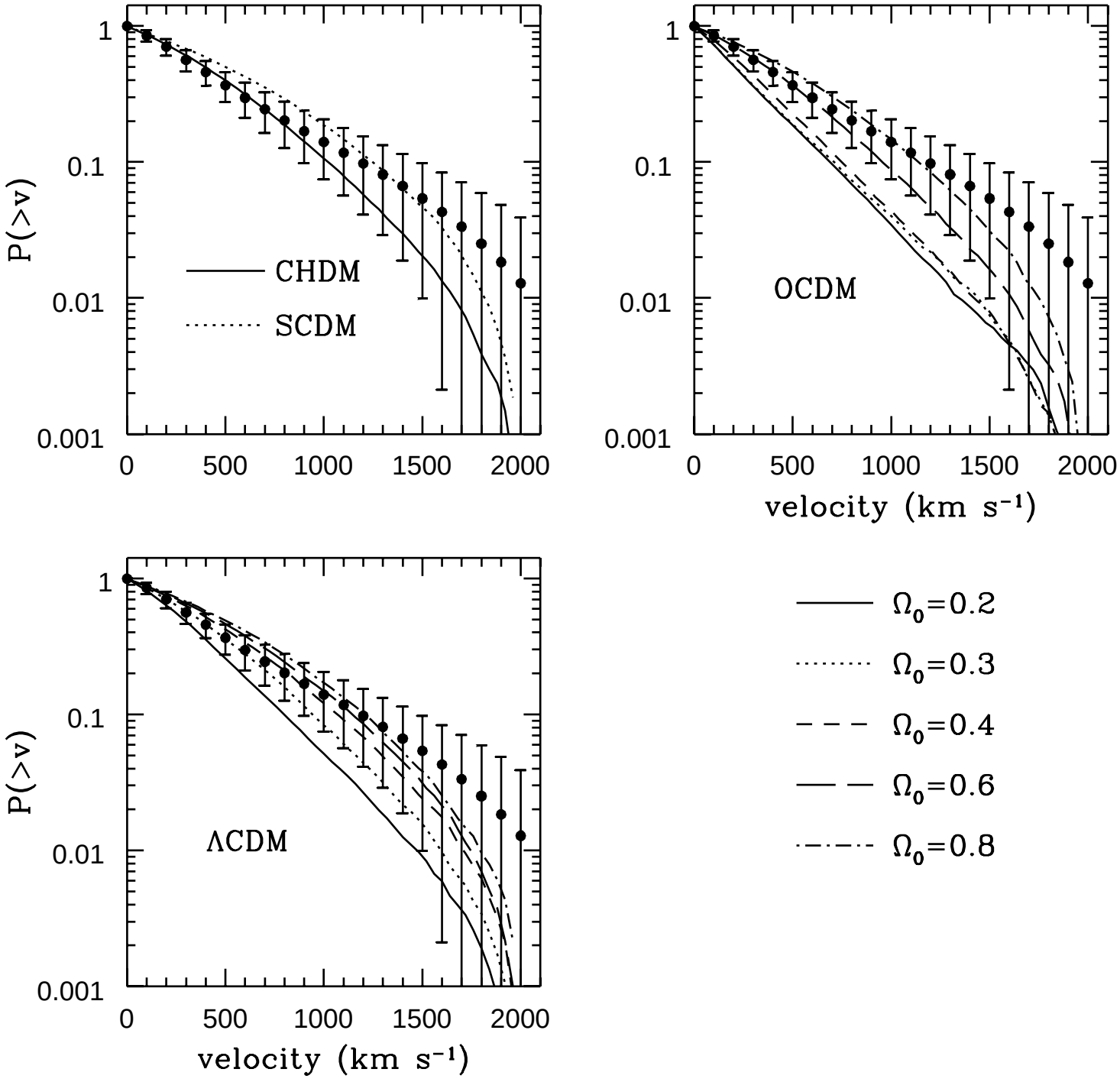
P(>v)
1
0.1
0.01
0.001
0
500
1000
1500
2000
CHDM
SCDM
OCDM
ΛCDM
velocity (km s⁻¹)
Ω₀=0.2
Ω₀=0.3
Ω₀=0.4
Ω₀=0.6
Ω₀=0.8